



**HAL**  
open science

# A macroscopic model including membrane exchange for diffusion MRI

Julien Coatléven, Housseem Haddar, Jing-Rebecca Li

► **To cite this version:**

Julien Coatléven, Housseem Haddar, Jing-Rebecca Li. A macroscopic model including membrane exchange for diffusion MRI. SIAM Journal on Applied Mathematics, 2013. hal-00768732v3

**HAL Id: hal-00768732**

**<https://inria.hal.science/hal-00768732v3>**

Submitted on 23 Mar 2013 (v3), last revised 25 Jan 2014 (v4)

**HAL** is a multi-disciplinary open access archive for the deposit and dissemination of scientific research documents, whether they are published or not. The documents may come from teaching and research institutions in France or abroad, or from public or private research centers.

L'archive ouverte pluridisciplinaire **HAL**, est destinée au dépôt et à la diffusion de documents scientifiques de niveau recherche, publiés ou non, émanant des établissements d'enseignement et de recherche français ou étrangers, des laboratoires publics ou privés.

# A MACROSCOPIC MODEL INCLUDING MEMBRANE EXCHANGE FOR DIFFUSION MRI

JULIEN COATLÉVEN\*, HOUSSEM HADDAR†, AND JING-REBECCA LI‡

**Abstract.** Diffusion Magnetic Resonance Imaging (dMRI) is a promising tool to obtain useful information on microscopic structure and has been extensively applied to biological tissues. We establish a new macroscopic model from homogenization theory to obtain the aggregate dMRI signal in the case of intermediate water exchange across cellular membranes. Based on a particular scaling of the permeability condition modeling cellular membranes, this model accurately reproduces the memory effects observed in practice. Explicit formulae given by homogenization for the coefficients of this model emphasize their link to the relevant physiological quantities, and the inverse problem of retrieving these coefficients from a set of measurements is considered. For dMRI signal modelling we are also able to reduce the obtained model to an ODE model that is more tractable for inversion. We discuss and numerically validate our model for physically relevant parameters.

**1. Introduction.** Diffusion Magnetic Resonance Imaging (dMRI) relies on the measurement of the diffusion (random motion due to thermal agitation) of water molecules in the imaged sample. If the imaged sample is biological tissue (for a survey, see [13]), it can be used to detect, for example, cerebral ischemia [21], demyelinating disorders[11], and tumors [16, 18, 20]. The signal measured by the MRI scanner is a mean-value measurement of the water proton magnetization in a physical volume whose size is much larger than the scale of the microscopic variations of the cellular structure. In fact, dMRI is used to show variations in the tissue structure on the macroscopic scale.

Unfortunately, there is a lack of accurate macroscopic models for dMRI in heterogeneous media in the presence of permeable cell membranes, with the exception of the Karger model [12], which was originally developed for micro-porous crystallites. The Karger model was obtained on the basis of phenomenological modeling of the experimentally obtained curves and only works under a strong and often unrealistic assumption on the applied diffusion-encoding magnetic field.

In this paper, starting from the complete description of the diffusion phenomenon at the microscopic level, which mathematically takes the form of a Bloch-Torrey PDE in a heterogeneous medium with barriers, varying at the scale of the biological cells, we will provide a macroscopic limit model, through homogenization, that is applicable to general diffusion-encoding magnetic fields. The main difficulty in the modeling of diffusion at the microscopic level is the choice of the membrane law. We adopted here the so-called two compartment model where the membrane is infinitesimal and induces a discontinuity of the field proportional to the flux. The nature of the homogenized model then would depend on the scaling for the proportionality coefficient with respect to the periodicity size parameter. A comprehensive presentation as well as a fully rigorous mathematical justification of all the possible limit models is the subject of a forthcoming work [6]. We will concentrate in this article on the relevant case for dMRI, i.e. the scaling that provides the limit model which fits best observed memory effects in experimental behavior.

We shall restrict ourselves to only a formal derivation of the homogenized model and put more emphasis on the application of this model to dMRI settings. Let us quote that the signal associated to this new macroscopic (and homogeneous) model, being the limit, when the size of biological cells tends to zero, of the real signal, is thus expected to be an approximation of the non-homogenized one at long diffusion times. The equations governing this signal will be of course much simpler than those involving the microscopic description of the medium. Their coefficients can be explicitly linked, in the context of periodic homogenization, to relevant properties of the underlying biological tissue. The reason we use periodic homogenization is that it is well known that even for media that are not truly periodic, the homogenized limit obtained in the periodic case remains formally relevant for describing the generic case (see for instance [1] and [2] for the case of porous media), i.e. the macroscopic equations remains of the same analytical form (only the exact values of the coefficients

---

\*INRIA Saclay Ile de France / Ecole Polytechnique (CMAP), Route de Saclay, 91128, Palaiseau France

†INRIA Saclay Ile de France / Ecole Polytechnique (CMAP), Route de Saclay, 91128, Palaiseau France

‡INRIA Saclay Ile de France / Ecole Polytechnique (CMAP), Route de Saclay, 91128, Palaiseau France

change).

For dMRI signal modelling we are also able to reduce the homogenized model to an ODE model that is more tractable for inversion. The Karger model can be seen as an approximate version of our model when the signal duration is very small. The main interest of this ODE model is indeed for the inverse problem of identifying the coefficients that make our approximate signal fit best the measured signal. Some preliminary inversion tests are performed on synthetic examples but with physically relevant parameters.

The paper will be organized as follows. In Section 2, we review the Bloch-Torrey PDE with barriers that accurately describes the dynamics involved in dMRI experiments at the microscopic level. For simplicity, we then make the hypothesis that the medium is periodic, to allow us to apply periodic homogenization theory. In Section 3, we make the formal homogenization of our model problem in the periodic context, using a particular scaling for the permeability condition on the cellular membranes. In Section 4, we provide an ODE description of the measured signal. We then show with a few numerical experiments that the signal from the homogenized model accurately approximates the full signal at long diffusion times. Finally, in Section 5 we solve numerically the inverse problem of finding the coefficients of our ODE model from the signal obtained without homogenization, and show that through these coefficients we can recover some relevant biological properties of the tissue.

**2. Model Problem.** Biological tissues contain abundant water and are composed of cells of various sizes and shapes surrounded by the extra-cellular space. The cells can be represented, at the scale of interest for our problem, as a bounded domain surrounded by a very thin membrane (see Figure 2.1 left). The diffusion coefficients for water in the interior part of the cell, in the membrane,

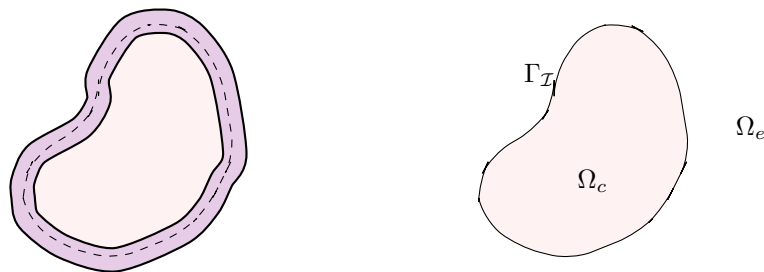


FIG. 2.1. Schematic of a biological cell, with its membrane (left) and an idealized two-compartment cell (right).

and in the extra-cellular space may be different from each other.

While the diffusion coefficients in the interior part of the cell and in the extra-cellular space remain of the same order of magnitude, it is much smaller inside the membrane. It is in fact extremely difficult to obtain direct measurements of this coefficient inside the cellular membrane, as this membrane is extremely thin. This is why the membrane is most of the time spatially neglected and replaced by a permeability condition between the extra-cellular and intra-cellular parts [15]. Consequently, we replace the realistic, "three-compartment" biological cell by the idealized "two-compartment" cell displayed in Figure 2.1 (right). For an imaging volume  $\Omega$  of biological tissue, we denote by  $\Gamma_{\mathcal{I}}$  the union of the boundaries of all the "two-compartment" cells included in  $\Omega$ .  $\Gamma_{\mathcal{I}}$  thus delimits two subdomains: the extracellular domain  $\Omega_e$  ( $e$  standing for extra-cellular) and the intra-cellular domain  $\Omega_c$  ( $c$  standing for cellular). The domain  $\Omega_{ext}$  then represents the union of the open extra-cellular and open intra-cellular domains, i.e.

$$\Omega_{ext} = \Omega \setminus \Gamma_{\mathcal{I}} = \Omega_e \cup \Omega_c$$

A classic dMRI experiment consists of applying two pulsed (meaning short duration in time) gradient (meaning linearly varying in space) magnetic fields with a 180 degree spin reversal in between the two in order to mark the positions of the water molecules between the two pulses [17].

The water magnetization  $M$  is modeled by the following Bloch-Torrey PDE [19] with jump

$$\begin{aligned}
\frac{\partial M(\mathbf{x}, t)}{\partial t} + \nu \mathbf{q} \cdot \mathbf{x} f(t) M(\mathbf{x}, t) - \operatorname{div}(\sigma(x) \nabla M(\mathbf{x}, t)) &= 0 && \text{in } \Omega_{ext} \times ]0, T[ \\
\sigma \nabla M \cdot \nu|_{\Gamma_{\mathcal{I}}} &= \kappa [M]|_{\Gamma_{\mathcal{I}}} && \text{on } \Gamma_{\mathcal{I}} \\
[\sigma \nabla M \cdot \nu]|_{\Gamma_{\mathcal{I}}} &= 0 && \text{on } \Gamma_{\mathcal{I}} \\
M(\cdot, 0) &= M_{init} && \text{in } \Omega_{ext}
\end{aligned}$$

where  $\nu$  is the normal exterior to the intra-cellular domains,  $[\cdot]_{\Gamma_{\mathcal{I}}}$  is the jump (extra-cellular minus intra-cellular) on  $\Gamma_{\mathcal{I}}$  for a quantity defined on both parts of the domain,  $\kappa$  is the permeability coefficient,  $\nu = \sqrt{-1}$ ,  $M_{init}$  is the initial magnetization. The constant vector in  $\mathbb{R}^d$ ,  $\mathbf{q}$ , contains the amplitude and direction of the applied magnetic field and the gyro-magnetic ratio of the water proton, and  $f$ , where  $\max_t f(t) = 1$ , is the normalized time profile of the diffusion-encoding magnetic field. The coefficient  $\sigma$  is the diffusion coefficient for water. The time profile of the classic Pulsed Gradient Spin Echo (PGSE) [17] sequence is the following:

$$\begin{cases} f(t) = 1, & 0 < t \leq \delta; \\ f(t) = -1, & \Delta < t \leq \Delta + \delta; \\ f(t) = 0, & \text{elsewhere;} \end{cases} \quad (2.1)$$

where we made  $f(t)$  negative in the second pulse to include the effect of the 180 degree spin reversal between the pulses. The time at which the signal is measured is called the echo time  $TE > \delta + \Delta$ .

For simplicity and in order to be able to apply a well known theoretical framework, we will assume that the imaging volume  $\Omega$  can be described as a periodic domain. More precisely, we will assume that there exists a period  $\varepsilon$ , which represents the average size of a "representative" volume of the full imaging volume, and will be assumed to be small compared to the size of  $\Omega$ .

We now define the unit periodicity cell  $Y = ]0, 1[^d$  such that  $Y = Y_e \cup Y_c$ , where  $Y_c$  is the intracellular domain, and is an open set which can be made of several connected parts (i.e it is the union of the interiors of the selection of biological cells that are included in the periodicity cell). Let  $N_c$  be the number of connected components of  $Y_c$ . Then we write  $Y_c = \bigcup_{i=1}^{N_c} Y_{c,i}$ . In the same way, for the extracellular domain  $Y_e$ , we write  $Y_e = \bigcup_{i=1}^{N_e} Y_{e,i}$  where  $N_e$  is the number of connected components of  $Y_e$ . If some cells touch each other and isolate a part of  $Y_e$ , then  $N_e \neq 1$ . We assume for simplicity that the boundary  $\partial Y_c$  of  $Y_c$  does not crosses  $\partial Y$  and we denote it  $\Gamma_m = \partial Y_c = \partial Y_e \setminus \partial Y$ . The general case can be treated in exactly the same way, but the geometrical description is more complicated: indeed, if  $\Gamma_m$  crosses  $\partial Y$ , then the biological cell must be periodically closed by another component of  $Y_c$  on the opposite side of  $\partial Y$ , so that the periodized domain only contains biological cells completely surrounded by membranes.

Now, we denote

$$\Xi_\varepsilon = \{ \xi \in \mathbb{Z}^d \mid \varepsilon(\xi + Y) \cap \Omega \neq \emptyset \}$$

so that  $\Omega$  will contain almost  $\#\{\Xi_\varepsilon\}$  periodicity cells. Finally, we denote

$$\overline{\Omega}_e^\varepsilon = \bigcup_{\xi \in \Xi_\varepsilon} \varepsilon(\xi + \overline{Y_e}) \cap \overline{\Omega}, \quad \Omega_c^\varepsilon = \bigcup_{\xi \in \Xi_\varepsilon} \varepsilon(\xi + Y_c) \cap \Omega, \quad \Omega_{ext}^\varepsilon = \Omega_e^\varepsilon \cup \Omega_c^\varepsilon. \quad (2.2)$$

Notice that

$$\partial \Omega_c^\varepsilon \cap \partial \Omega_e^\varepsilon = \partial \Omega_e^\varepsilon \setminus \partial \overline{\Omega} = \bigcup_{\xi \in \Xi_\varepsilon} \Gamma_m^{\varepsilon, \xi} \quad \text{where} \quad \Gamma_m^{\varepsilon, \xi} = \varepsilon(\xi + \Gamma_m) \cap \Omega.$$

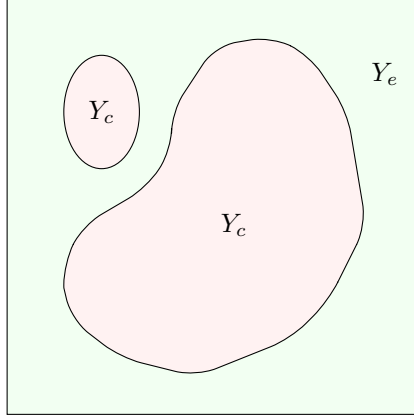


FIG. 2.2. A periodicity cell  $Y$ , containing simplified biological cells with an infinitely thin interface for membrane

Of course, the diffusion coefficient will be assumed to be periodic as well, i.e there exists  $\hat{\sigma} \in L^\infty(Y)$  such that  $\sigma(x) = \hat{\sigma}\left(\frac{x}{\varepsilon}\right)$ , with

$$\hat{\sigma} = \begin{cases} \sigma_c & \text{in } Y_c \\ \sigma_e & \text{in } Y_e \end{cases} \quad (2.3)$$

The most common practical choice for  $\sigma_e$  and  $\sigma_c$  is to take them constant, so that  $\hat{\sigma}$  is piecewise constant. For both physical and technical reasons, we will further assume that there exists two constants  $0 < \sigma^- < \sigma^+ < +\infty$  such that, for almost every  $y \in Y$

$$\sigma^- \leq \sigma_c \leq \sigma^+ \quad \text{and} \quad \sigma^- \leq \sigma_e \leq \sigma^+$$

With these more precise description of the domain, our model problem can be rewritten as

$$\begin{cases} \frac{\partial M_\varepsilon(\mathbf{x}, t)}{\partial t} + \nu \mathbf{q} \cdot \mathbf{x} f(t) M_\varepsilon(\mathbf{x}, t) - \text{div}(\hat{\sigma}_\varepsilon(x) \nabla M_\varepsilon(\mathbf{x}, t)) = 0 & \text{in } \Omega_{ext}^\varepsilon \times ]0, T[ \\ \hat{\sigma}_\varepsilon \nabla M_\varepsilon \cdot \nu|_{\Gamma_m^{\varepsilon, \xi}} = \kappa^\varepsilon [M_\varepsilon]|_{\Gamma_m^{\varepsilon, \xi}} & \forall \xi \in \Xi_\varepsilon \\ [\hat{\sigma}_\varepsilon \nabla M_\varepsilon \cdot \nu]|_{\Gamma_m^{\varepsilon, \xi}} = 0 & \forall \xi \in \Xi_\varepsilon \\ M_\varepsilon(\cdot, 0) = M_{init} & \text{in } \Omega_{ext}^\varepsilon \end{cases} \quad (2.4)$$

where  $\hat{\sigma}_\varepsilon = \hat{\sigma}\left(\frac{x}{\varepsilon}\right)$ . Finally, we will assume that the time profile  $f$  belongs to  $L^\infty(]0, T[)$  and that the initial data  $M_{init}$  is defined on  $\Omega$  independently of  $\varepsilon$  and belongs to  $L^2(\Omega) \cap L^1(\Omega)$ . For notation convenience we set  $Q(\mathbf{x}) := \mathbf{q} \cdot \mathbf{x}$ .

It only remains to choose the domain  $\Omega$  itself. We want to model an imaging volume at the scale of the spatial resolution of dMRI (usually on the order of  $1 \text{ mm}^3$ ). However, because the magnetic fields are applied to the entire probed sample, two imaging volumes that have a common boundary will exchange water during the experiment. But the influence of this exchange will be small because the aggregate diffusion coefficient of water in biological tissue is at most  $10^{-3} \text{ mm}^2/\text{s}$ , meaning even for the longest diffusion times (corresponding to  $\Delta$  around  $100 \text{ ms}$ ), the diffusion distance will be no more than  $25 \mu\text{m}$ , much smaller than the length across an imaging volume. Hence, a very small percentage of the water molecules come from a neighboring imaging volume or have left for a neighboring imaging volume during the dMRI experiment. Thus their influence to the aggregate magnetization in a particular imaging volume can be neglected.

From the mathematical point of view, using the linearity of the equation as well as its parabolic nature, we can say that an initial condition supported in a given imaging volume will give birth to a contribution that will be exponentially decaying in the space outside the imaging volume. Thus, the measured signal in a imaging volume is only minorly influenced by the surrounding imaging volumes and not at all by imaging volumes further away. Hence we are allowed to extend our imaging volume by periodic copies of itself instead of its actual neighboring imaging volumes. Thus, it is reasonable to consider as a good approximation that we can pose our problem by extending the imaging volume of interest to  $\Omega = \mathbb{R}^d$  which contains infinitely many periodic copies of the imaging volume of interest. Given that the spatial variations between neighboring imaging volumes are not too big in biological imaging applications, we believe that this periodic extension of the imaging volume of interest to all of  $\mathbb{R}^d$  is a reasonable approximation. We note that the homogenized limit we are going to obtain would have been the same if we had considered a bounded domain with Neumann or Dirichlet boundary conditions (with the modification that the boundary conditions would then apply also to the homogenized limit).

Finally, we conclude this section by explaining our choice for the permeability coefficient  $\kappa^\varepsilon$ . As usual in homogenization, the choice of a scaling for this coefficient, driven by the fact that it is experimentally a very small parameter, will be determinant with regard to the limit model. More precisely the dependence of  $\kappa^\varepsilon$  on  $\varepsilon \rightarrow 0$  will influence the nature of the the limit macroscopic model. A comprehensive presentation as well as a fully rigorous mathematical justification of all the possible limit models corresponding to a scaling  $\kappa^\varepsilon = \sigma_m \varepsilon^m$  for all  $m \in \mathbb{Z}$  is the subject of a forthcoming work [6]. We will concentrate in this article on the relevant case for dMRI, i.e. the scaling that provides the limit model which fits best observed experimental behavior, and which corresponds with  $m = 1$ . We shall restrict ourselves to only a formal derivation of the homogenized model and put more emphasis on the application of this model to dMRI settings.

**3. A macroscopic model through two scale asymptotic expansions.** In this section, we derive our macroscopic model through formal homogenization from the two compartment model. We note here that  $M_\varepsilon$  does not satisfy the Bloch-Torrey equation in all  $\Omega_{ext}^\varepsilon$ , but separately in  $\Omega_c^\varepsilon$  and  $\Omega_e^\varepsilon$ , with jump conditions on the  $\Gamma_m^{\varepsilon,\xi}$ 's. This remark will be important to our formal derivation of the macroscopic models.

**3.1. Formal derivation of the macroscopic models through two-scale asymptotic expansions.** Using classical periodic homogenization techniques [3], we are going to develop  $M_\varepsilon$  using two-scale asymptotic expansions. According to our previous remark, we are not going to introduce a unique expansion in all  $\Omega_{ext}^\varepsilon$ , but two expansions, one for each phase  $\Omega_c^\varepsilon$  and  $\Omega_e^\varepsilon$ . Consequently, we write

$$\left\{ \begin{array}{l} M_\varepsilon(\mathbf{x}, t) = M_\varepsilon^e(\mathbf{x}, t) = \sum_{i=0}^{+\infty} \varepsilon^i M_{i,e} \left( \mathbf{x}, \frac{\mathbf{x}}{\varepsilon}, t \right) \quad \text{in } \Omega_e^\varepsilon \\ M_\varepsilon(\mathbf{x}, t) = M_\varepsilon^c(\mathbf{x}, t) = \sum_{i=0}^{+\infty} \varepsilon^i M_{i,c} \left( \mathbf{x}, \frac{\mathbf{x}}{\varepsilon}, t \right) \quad \text{in } \Omega_c^\varepsilon \end{array} \right. \quad (3.1)$$

where the functions  $M_{i,e}(\mathbf{x}, y, t)$  and  $M_{i,c}(\mathbf{x}, y, t)$  are defined respectively on  $\Omega \times Y_e \times ]0, T[$  and  $\Omega \times Y_c \times ]0, T[$ , and the  $M_{i,e}(\mathbf{x}, y, t)$  are assumed  $Y$ -periodic in  $y$ . The aim of such an ansatz is to separate the "macroscopic" variations (the  $\mathbf{x}$  variable) from the "microscopic" ones (the  $y$  variable), and then try to obtain a new problem involving only the macroscopic one.

**3.1.1. Periodicity cell equations and jump conditions.** To get the equations for each of the  $M_{i,e}$ 's and the  $M_{i,c}$ 's, we start by noticing that,  $\alpha \in \{c, e\}$ ,

$$\nabla M_{i,\alpha} \left( \mathbf{x}, \frac{\mathbf{x}}{\varepsilon}, t \right) = \nabla_{\mathbf{x}} M_{i,\alpha} \left( \mathbf{x}, \frac{\mathbf{x}}{\varepsilon}, t \right) + \varepsilon^{-1} \nabla_y M_{i,\alpha} \left( \mathbf{x}, \frac{\mathbf{x}}{\varepsilon}, t \right),$$

and therefore

$$\begin{aligned} \operatorname{div} \left( \sigma_\alpha \left( \frac{\mathbf{x}}{\varepsilon} \right) \nabla M_{i,\alpha}(\mathbf{x}, \frac{\mathbf{x}}{\varepsilon}, t) \right) &= \operatorname{div}_{\mathbf{x}} \left( \sigma_\alpha \left( \frac{\mathbf{x}}{\varepsilon} \right) \nabla_{\mathbf{x}} M_{i,\alpha}(\mathbf{x}, \frac{\mathbf{x}}{\varepsilon}, t) \right) + \varepsilon^{-2} \operatorname{div}_y \left( \sigma_\alpha \left( \frac{\mathbf{x}}{\varepsilon} \right) \nabla_y M_{i,\alpha}(\mathbf{x}, \frac{\mathbf{x}}{\varepsilon}, t) \right) \\ &+ \varepsilon^{-1} \operatorname{div}_{\mathbf{x}} \left( \sigma_\alpha \left( \frac{\mathbf{x}}{\varepsilon} \right) \nabla_y M_{i,\alpha}(\mathbf{x}, \frac{\mathbf{x}}{\varepsilon}, t) \right) + \varepsilon^{-1} \operatorname{div}_y \left( \sigma_\alpha \left( \frac{\mathbf{x}}{\varepsilon} \right) \nabla_{\mathbf{x}} M_{i,\alpha}(\mathbf{x}, \frac{\mathbf{x}}{\varepsilon}, t) \right) \end{aligned}$$

Plugging these formulae into the two compartment model, using the asymptotic expansions (3.1) then matching the terms in front of the same power of  $\varepsilon$ , one gets for the three first orders,

$$-\operatorname{div}_y (\sigma_\alpha \nabla_y M_{0,\alpha}) = 0 \quad \text{in } \Omega \times Y_\alpha \times ]0, T[, \quad (3.2)$$

$$-\operatorname{div}_y (\sigma_\alpha \nabla_y M_{1,\alpha}) = \operatorname{div}_y (\sigma_\alpha \nabla_{\mathbf{x}} M_{0,\alpha}) + \operatorname{div}_{\mathbf{x}} (\sigma_\alpha \nabla_y M_{0,\alpha}) \quad \text{in } \Omega \times Y_\alpha \times ]0, T[, \quad (3.3)$$

$$\begin{aligned} -\operatorname{div}_y (\sigma_\alpha \nabla_y M_{2,\alpha}) &= \operatorname{div}_y (\sigma_\alpha \nabla_{\mathbf{x}} M_{1,\alpha}) - \operatorname{div}_{\mathbf{x}} (\sigma_\alpha (\nabla_y M_{1,\alpha} + \nabla_{\mathbf{x}} M_{0,\alpha})) \\ &- \frac{\partial M_{0,\alpha}}{\partial t} - \iota Q f(t) M_{0,\alpha} \quad \text{in } \Omega \times Y_\alpha \times ]0, T[. \end{aligned} \quad (3.4)$$

Notice that the equations have been formally expanded to all  $\Omega$  for the macroscopic variable  $\mathbf{x}$ . Next, we make the following ansatz for the jumps of  $M_\varepsilon$  and its fluxes, for  $\mathbf{x} \in \Gamma_m^\varepsilon$ ,

$$[M_\varepsilon]_{|\Gamma_m^\varepsilon}(\mathbf{x}, t) = \sum_{i=0}^{\infty} \varepsilon^i \left( M_{i,e}(\mathbf{x}, \frac{\mathbf{x}}{\varepsilon}, t) - M_{i,c}(\mathbf{x}, \frac{\mathbf{x}}{\varepsilon}, t) \right) \quad (3.5)$$

$$[\hat{\sigma}_\varepsilon \nabla M_\varepsilon \cdot \nu]_{|\Gamma_m^\varepsilon} = \sum_{i=0}^{\infty} \varepsilon^i \left( \sigma_e \nabla M_{i,e}(\mathbf{x}, \frac{\mathbf{x}}{\varepsilon}, t) \cdot \nu - \sigma_c \nabla M_{i,c}(\mathbf{x}, \frac{\mathbf{x}}{\varepsilon}, t) \cdot \nu \right) \quad (3.6)$$

Then, the no-jump relation for the fluxes becomes

$$\begin{aligned} \varepsilon^{-1} (\sigma_e \nabla_y M_{0,e} \cdot \nu - \sigma_c \nabla_y M_{0,c} \cdot \nu) \\ + \sum_{i=0}^{\infty} \varepsilon^i (\sigma_e \nabla_y M_{i+1,e} \cdot \nu + \sigma_e \nabla_{\mathbf{x}} M_{i,e} \cdot \nu - \sigma_c \nabla_y M_{i+1,c} \cdot \nu - \sigma_c \nabla_{\mathbf{x}} M_{i,c} \cdot \nu) = 0, \end{aligned}$$

which gives, after identifying each power of  $\varepsilon$  and expanding to all  $(\mathbf{x}, y) \in \Omega \times \Gamma_m$

$$\sigma_e \nabla_y M_{0,e} \cdot \nu = \sigma_c \nabla_y M_{0,c} \cdot \nu \quad \text{in } \Omega \times \Gamma_m \times ]0, T[, \quad (3.7)$$

and for  $i \geq 1$ ,

$$\sigma_e \nabla_y M_{i,e} \cdot \nu + \sigma_e \nabla_{\mathbf{x}} M_{i-1,e} \cdot \nu = \sigma_c \nabla_y M_{i,c} \cdot \nu + \sigma_c \nabla_{\mathbf{x}} M_{i-1,c} \cdot \nu \quad \text{in } \Omega \times \Gamma_m \times ]0, T[. \quad (3.8)$$

To write the equivalent condition for the traces, recall that we have assumed that  $\kappa^\varepsilon = \varepsilon \sigma_m$ , where  $\sigma_m > 0$  is a constant independent on  $\varepsilon$ . Now we write the jump relations for traces, using (3.7) and (3.8) as

$$\begin{aligned} \sum_{i=0}^{+\infty} \varepsilon^{i+1} \sigma_m (M_{i,e} - M_{i,c}) &= \varepsilon^{-1} \sigma_\alpha \nabla_y M_{0,\alpha} \cdot \nu + \varepsilon^0 \sigma_\alpha (\nabla_y M_{1,\alpha} \cdot \nu + \nabla_{\mathbf{x}} M_{0,\alpha} \cdot \nu) \\ &+ \varepsilon^1 \sigma_\alpha (\nabla_y M_{2,\alpha} \cdot \nu + \nabla_{\mathbf{x}} M_{1,\alpha} \cdot \nu) + \sum_{i=2}^{+\infty} \varepsilon^i \sigma_\alpha (\nabla_y M_{i+1,\alpha} \cdot \nu + \nabla_{\mathbf{x}} M_{i,\alpha} \cdot \nu). \end{aligned}$$

**3.1.2. Formal limit problem.** As usual when performing formal homogenization through two-scale asymptotic expansions, we only need (as we shall see) to obtain the equations for the first three terms,  $M_{0,\alpha}$ ,  $M_{1,\alpha}$  and  $M_{2,\alpha}$ . The problem for  $M_{0,\alpha}$  is then given by

$$\left\{ \begin{array}{l} -\operatorname{div}_y(\sigma_\alpha \nabla_y M_{0,\alpha}) = 0 \quad \text{in } Y_\alpha, \\ \sigma_\alpha \nabla_y M_{0,\alpha} \cdot \nu = 0 \quad \text{on } \Gamma_m, \\ M_{0,\alpha} \text{ is } Y\text{-periodic.} \end{array} \right. \quad (3.9)$$

Let us recall the following classical lemma (see for instance [3, 4]) on solutions to this type of problems that will also be useful to derive the macroscopic model.

LEMMA 1. *Let  $f_c \in L^2(Y_c)$ ,  $f_e \in L^2(Y_e)$ ,  $\psi_c$  and  $\psi_e \in H^{-1/2}(\Gamma_m)$ . Then, there exists a unique solution  $u_c \in H^1(Y_c)$ , up to a constant, to*

$$\left\{ \begin{array}{l} -\operatorname{div}_y(\sigma_c \nabla_y u_c) = f_c \quad \text{in } Y_c, \\ \sigma_c \nabla_y u_c \cdot \nu = \psi_c \quad \text{on } \Gamma_m, \end{array} \right.$$

if and only if, for any  $i \in \llbracket 1, N_c \rrbracket$ ,  $\int_{Y_{c,i}} f_c + \langle \psi_c, 1 \rangle_{H^{-1/2}(\Gamma_m \cap \partial Y_{c,i}), H^{1/2}(\Gamma_m \cap \partial Y_{c,i})} = 0$ , and there exists a unique solution  $u_e \in H_{\#}^1(Y_e)$ , up to a constant, to

$$\left\{ \begin{array}{l} -\operatorname{div}_y(\sigma_e \nabla_y u_e) = f_e \quad \text{in } Y_e, \\ \sigma_e \nabla_y u_e \cdot \nu = \psi_e \quad \text{on } \Gamma_m, \\ u_e \text{ } Y\text{-periodic,} \end{array} \right.$$

if and only if, for any  $i \in \llbracket 1, N_e \rrbracket$ ,  $\int_{Y_{e,i}} f_e - \langle \psi_e, 1 \rangle_{H^{-1/2}(\Gamma_m \cap \partial Y_{e,i}), H^{1/2}(\Gamma_m \cap \partial Y_{e,i})} = 0$ , where  $H_{\#}^1(Y_e)$  is the space of  $H^1$  and  $Y$ -periodic functions on  $Y_e$ . The above lemma tells us that neither  $M_{0,e}$  nor  $M_{0,c}$  depend on  $y$ . The problem for  $M_{1,\alpha}$  is consequently

$$\left\{ \begin{array}{l} -\operatorname{div}_y(\sigma_\alpha (\nabla_y M_{1,\alpha} + \nabla_{\mathbf{x}} M_{0,\alpha})) = 0 \quad \text{in } Y_\alpha, \\ \sigma_\alpha \nabla_y M_{1,\alpha} \cdot \nu + \sigma_\alpha \nabla_{\mathbf{x}} M_{0,\alpha} \cdot \nu = 0 \quad \text{on } \Gamma_m, \\ M_{1,\alpha} \text{ is } Y\text{-periodic in the } y \text{ variable.} \end{array} \right. \quad (3.10)$$

Thus, introducing for  $i = 1, d$  the cell problems

$$\left\{ \begin{array}{l} -\operatorname{div}_y(\sigma_\alpha (\nabla_y w_{i,\alpha} + e_i)) = 0 \quad \text{in } Y_\alpha, \\ \sigma_\alpha \nabla_y w_{i,\alpha} \cdot \nu + \sigma_\alpha e_i \cdot \nu = 0 \quad \text{on } \Gamma_m, \\ w_{i,\alpha} \text{ is } Y\text{-periodic,} \end{array} \right. \quad (3.11)$$

which are well posed (in appropriate  $H^1$  spaces) according to Lemma 1 since, using the divergence theorem,

$$\int_{Y_c} \operatorname{div}_y \sigma_c e_i dy - \int_{\Gamma_m} \sigma_c e_i \cdot \nu ds = \int_{Y_c} \operatorname{div}_y \sigma_e e_i dy + \int_{\Gamma_m} \sigma_e e_i \cdot \nu ds = 0, \quad (3.12)$$

one can express the solutions to (3.10) as

$$M_{1,\alpha} = \sum_{i=1}^d w_{i,\alpha} \frac{\partial M_{0,\alpha}}{\partial \mathbf{x}_c} \quad \text{in } Y_\alpha. \quad (3.13)$$

Now, we consider the equations satisfied by  $M_{2,\alpha}$  where the variables  $\mathbf{x}$  and  $t$  are treated as parameters.

$$\left\{ \begin{array}{ll} -\operatorname{div}_y(\sigma_\alpha(\nabla_y M_{2,\alpha} + \nabla_{\mathbf{x}} M_{1,\alpha})) = \operatorname{div}_{\mathbf{x}}(\sigma_\alpha(\nabla_y M_{1,\alpha} + \nabla_{\mathbf{x}} M_{0,\alpha})) - \frac{\partial M_{0,\alpha}}{\partial t} - \imath Qf(t)M_{0,\alpha} & \text{in } Y_\alpha, \\ \sigma_e \nabla_y M_{2,e} \cdot \nu + \sigma_e \nabla_{\mathbf{x}} M_{1,e} \cdot \nu = \sigma_m(M_{0,e} - M_{0,c}) & \text{on } \Gamma_m, \\ \sigma_c \nabla_y M_{2,c} \cdot \nu + \sigma_c \nabla_{\mathbf{x}} M_{1,c} \cdot \nu = \sigma_m(M_{0,e} - M_{0,c}) & \text{on } \Gamma_m, \\ M_{2,e} \text{ is } Y\text{-periodic in the } y \text{ variable.} & \end{array} \right. \quad (3.14)$$

Using lemma 1, it is easy to see that the compatibility condition for  $M_{2,e}$  implies

$$\int_{Y_e} \operatorname{div}_{\mathbf{x}}(\sigma_e(\nabla_y M_{1,e} + \nabla_{\mathbf{x}} M_{0,e})) - \frac{\partial M_{0,e}}{\partial t} - \imath Qf(t)M_{0,e} - \int_{\Gamma_m} \sigma_m(M_{0,e} - M_{0,c}) = 0, \quad (3.15)$$

while the compatibility condition for  $M_{2,c}$  implies

$$\int_{Y_c} \operatorname{div}_{\mathbf{x}}(\sigma_c(\nabla_y M_{1,c} + \nabla_{\mathbf{x}} M_{0,c})) - \frac{\partial M_{0,c}}{\partial t} - \imath Qf(t)M_{0,c} + \int_{\Gamma_m} \sigma_m(M_{0,e} - M_{0,c}) = 0. \quad (3.16)$$

We define the homogenized tensors  $D_\alpha$  through

$$D_{\alpha,ij} := \frac{1}{|Y_\alpha|} \int_{Y_e} \sigma_e \nabla w_{j,\alpha} \cdot e_i + \sigma_\alpha e_j \cdot e_i,$$

$i, j = 1, d$  which can be also expressed in a symmetric form

$$D_{\alpha,ij} = \frac{1}{|Y_\alpha|} \int_{Y_\alpha} \sigma_\alpha (\nabla w_{j,\alpha} + e_j) \cdot (\nabla w_{i,\alpha} + e_i) \quad (3.17)$$

since, using (3.11),

$$\int_{Y_\alpha} \sigma_\alpha (\nabla w_{j,\alpha} + e_j) \cdot \nabla w_{i,\alpha} = - \int_{Y_\alpha} \operatorname{div}_y(\sigma_\alpha (\nabla w_{j,\alpha} + e_j)) w_{i,\alpha} = 0.$$

We also define the two coefficients

$$\eta_c := \frac{\sigma_m |\Gamma_m|}{|Y_c|} \quad \text{and} \quad \eta_e := \frac{\sigma_m |\Gamma_m|}{|Y_e|}. \quad (3.18)$$

Then, using the fact that  $M_{0,e}$  and  $M_{0,c}$  does not depend on  $y$ , we obtain from (3.15) and (3.16) the macroscopic model

$$\left\{ \begin{array}{ll} \frac{\partial M_{0,e}}{\partial t} + \imath Qf(t)M_{0,e} - \operatorname{div}_{\mathbf{x}}(D_e \nabla_{\mathbf{x}} M_{0,e}) + \eta_e(M_{0,e} - M_{0,c}) = 0, & \text{in } \Omega \times ]0, T[ \\ M_{0,e}(\cdot, 0) = M_{init}, & \text{in } \Omega \\ \frac{\partial M_{0,c}}{\partial t} + \imath Qf(t)M_{0,c} - \operatorname{div}_{\mathbf{x}}(D_c \nabla_{\mathbf{x}} M_{0,c}) + \eta_c(M_{0,c} - M_{0,e}) = 0, & \text{in } \Omega \times ]0, T[ \\ M_{0,c}(\cdot, 0) = M_{init}, & \text{in } \Omega \end{array} \right. \quad (3.19)$$

which is a coupled system of modified Bloch-Torrey equations, with homogeneous diffusion tensors.

**3.2. A simplified macroscopic model.** For our setting of the problem where we assumed that  $Y_c$  does not touch the boundary of  $Y$  the homogenized system (3.19) can be simplified since in

that case  $D_c = 0$ . This can be easily seen by checking that  $w_{i,c} = -y_i$  and therefore  $\nabla_y w_{i,c} + e_i = 0$ . Consequently our model simplifies to

$$\left\{ \begin{array}{ll} \frac{\partial M_{0,e}}{\partial t} + \imath Q f(t) M_{0,e} - \operatorname{div}_{\mathbf{x}}(D_e \nabla_{\mathbf{x}} M_{0,e}) + \eta_e (M_{0,e} - M_{0,c}) = 0 & \text{in } \Omega \times ]0, T[, \\ M_{0,e}(\cdot, 0) = M_{init} & \text{in } \Omega, \\ \frac{\partial M_{0,c}}{\partial t} + \imath Q f(t) M_{0,c} + \eta_c (M_{0,c} - M_{0,e}) = 0 & \text{in } \Omega \times ]0, T[, \\ M_{0,c}(\cdot, 0) = M_{init} & \text{in } \Omega. \end{array} \right. \quad (3.20)$$

Remark that the equation for  $M_{0,c}$  can be solved in terms of  $M_{0,e}$

$$M_{0,c}(\mathbf{x}, t) = M_{init} G_c(\mathbf{x}, t, 0) + \int_0^t G_c(\mathbf{x}, t, s) M_{0,e}(\mathbf{x}, s) ds \quad (3.21)$$

where we have set

$$G_c(\mathbf{x}, t, s) := \exp\left(-\int_s^t (\imath \mathbf{q} \cdot \mathbf{x} f(r) + \eta_c) dr\right). \quad (3.22)$$

Thus, we can decouple the system (3.20) into

$$\left\{ \begin{array}{ll} \frac{\partial M_{0,e}}{\partial t} + (\imath Q f(t) + \eta_e) M_{0,e} - \operatorname{div}_{\mathbf{x}}(D_e \nabla_{\mathbf{x}} M_{0,e}) - \eta_e \int_0^t G_c(t, s) M_{0,e}(s) ds \\ = \eta_e M_{init} G_c(t) & \text{in } \Omega \times ]0, T[, \\ M_{0,e}(\cdot, 0) = M_{init} & \text{in } \Omega, \\ M_{0,c} = M_{init} G_c(t, 0) + \int_0^t G_c(t, s) M_{0,e}(s) ds & \text{in } \Omega \times ]0, T[. \end{array} \right. \quad (3.23)$$

The first equation of (3.23) emphasizes the fact that this macroscopic model will behave quite differently from a classical Bloch-Torrey equation. In particular, the presence of the integral with respect to time gives birth to memory effects for  $M_{0,e}$ . Let us also remark that since the boundary of  $Y$  is contained in the boundary of  $Y_e$ , then the homogenized tensor  $D_e$  is positive definite as soon as  $\sigma_c$  is also positive definite [3]. Then we can expect some well posedness of the homogenized problem. We recall that for simplicity we take  $\Omega = \mathbb{R}^d$ . With this choice, problem (3.20) involves an unbounded coefficient, namely  $Q(x)$ , and therefore its analysis is not classical. In particular, it is not clear in which sense problem (3.20) is to be understood. To make it more precise, we set  $\mathbf{q} = q\mathbf{n}$ , where  $\mathbf{n}$  is a unitary vector of  $\mathbb{R}^d$ , and define  $\widetilde{M}_\alpha$  almost everywhere on  $\mathbb{R}^d \times ]0, T[$ , for  $\alpha \in \{e, c\}$  by

$$\widetilde{M}_{0,\alpha}(x, t) = M_{0,\alpha}(x, t) e^{\imath q \mathbf{x} \cdot \mathbf{n} \int_0^t f(s) ds} \quad (3.24)$$

denoting  $q = q\mathbf{n}$ , where  $\mathbf{n}$  is a unitary vector. Then, at least formally, and with  $F(t) := \int_0^t f(s) ds$ ,

$$\frac{\partial \widetilde{M}_{0,\alpha}}{\partial t} = \left( \frac{\partial M_{0,\alpha}}{\partial t} + \imath q \mathbf{n} \cdot \mathbf{x} f(t) M_{0,\alpha} \right) e^{\imath q \mathbf{n} \cdot \mathbf{x} F(t)},$$

$$\nabla \widetilde{M}_{0,\alpha} = (\nabla M_{0,\alpha} + \imath q \mathbf{n} M_{0,\alpha} F(t)) e^{\imath q \mathbf{n} \cdot \mathbf{x} F(t)},$$

$$\operatorname{div}(D_\alpha \nabla \widetilde{M}_{0,\alpha}) = (\operatorname{div}(D_\alpha \nabla M_{0,\alpha}) + \imath q D_\alpha \nabla M_{0,\alpha} \cdot \mathbf{n} F(t)) e^{\imath q \mathbf{n} \cdot \mathbf{x} F(t)} + \operatorname{div}\left(\imath q D_\alpha \widetilde{M}_{0,\alpha} \cdot \mathbf{n} F(t)\right).$$

Then, since

$$\imath q D_\alpha \nabla M_{0,\alpha} \cdot \mathbf{n} F(t) e^{\imath q \mathbf{n} \cdot \mathbf{x} F(t)} = \imath q D_\alpha \nabla \widetilde{M}_{0,\alpha} \cdot \mathbf{n} F(t) + q^2 D_\alpha \widetilde{M}_{0,\alpha} F(t)^2,$$

we get

$$\operatorname{div}(D_\alpha \nabla \widetilde{M}_{0,\alpha}) = \operatorname{div}(D_\alpha \nabla M_{0,\alpha}) e^{\imath q \mathbf{n} \cdot \mathbf{x} F(t)} + \imath q D_\alpha \nabla \widetilde{M}_{0,\alpha} \cdot \mathbf{n} F(t) + q^2 D_\alpha F(t)^2 \widetilde{M}_{0,\alpha} + \operatorname{div}(\imath q D_\alpha \widetilde{M}_{0,\alpha} \cdot \mathbf{n} F(t)),$$

and finally obtain

$$\left\{ \begin{array}{l} \frac{\partial \widetilde{M}_{0,e}}{\partial t} - \operatorname{div}\left(D_e\left(\nabla \widetilde{M}_{0,e} - \imath q \mathbf{n} F(t) \widetilde{M}_{0,e}\right)\right) + \imath q D_e \nabla \widetilde{M}_{0,e} \cdot \mathbf{n} F(t) + q^2 D_e F(t)^2 \widetilde{M}_{0,e} \\ + \eta_e(\widetilde{M}_{0,e} - \widetilde{M}_{0,c}) = 0 \quad \text{in } \mathbb{R}^d \times ]0, T[ \\ \frac{\partial \widetilde{M}_{0,c}}{\partial t} + \eta_c(\widetilde{M}_{0,c} - \widetilde{M}_{0,e}) = 0 \quad \text{in } \mathbb{R}^d \times ]0, T[ \\ \widetilde{M}_{0,e}(\cdot, 0) = M_{init} \quad \text{in } \mathbb{R}^d \\ \widetilde{M}_{0,c}(\cdot, 0) = M_{init} \quad \text{in } \mathbb{R}^d \end{array} \right. \quad (3.25)$$

While it may seem a more complicated problem, notice that it does not involve any unbounded coefficients, and its analysis enters a well-known theoretical framework.

**THEOREM 1.** *Let  $f \in L^\infty(0, T)$  and  $M_{init} \in L^2(\Omega)$ . We denote  $H = L^2(\Omega) \times L^2(\Omega)$ ,  $X = H^1(\Omega) \times L^2(\Omega)$ ,  $X' = H^{-1}(\Omega) \times L^2(\Omega)$  and*

$$W(0, T, X) = \left\{ U \in L^2(0, T, X) \mid \partial_t U \in L^2(0, T, X') \right\}$$

*There exists a unique solution  $\widetilde{M} = (\widetilde{M}_e, \widetilde{M}_c) \in W(0, T, X) \cap C^0(0, T, L^2(\mathbb{R}^d))^2$  to problem (3.25) which moreover satisfies for some  $C, C' > 0$ ,*

$$\|\widetilde{M}\|_{L^\infty(0, T, H)} \leq \sqrt{2} e^{CT} \|M_{init}\|_H, \quad (3.26)$$

and

$$\|\widetilde{M}\|_{L^2(0, T, X)} \leq C' (1 + e^{CT}) \|M_{init}\|_H. \quad (3.27)$$

*Proof.* We denote  $\langle \cdot, \cdot \rangle_{H^{-1}, H^1}$  the duality product between  $H^{-1}(\mathbb{R})$  and  $H^1(\mathbb{R}^d)$  and  $(\cdot, \cdot)_{L^2}$  the scalar product on  $L^2(\mathbb{R}^d)$ . If there exists a solution  $\widetilde{M} \in W(0, T, X)$ , we can use any function  $V \in X$  as a test function for problem (3.25), and we get after formally integrating by parts

$$\left\{ \begin{array}{l} \left\langle \partial_t \widetilde{M}_{0,e}, V_e \right\rangle_{H^{-1}, H^1} + \left( D_e \nabla \widetilde{M}_{0,e}, \nabla V_e \right)_{L^2} + \left( \eta_e(\widetilde{M}_{0,e} - \widetilde{M}_{0,c}), V_e \right)_{L^2} - \left( \imath q F(t) D_e \widetilde{M}_{0,e} \mathbf{n}, \nabla V_e \right)_{L^2} \\ + \left( \imath q F(t) D_e \nabla \widetilde{M}_{0,e} \cdot \mathbf{n}, V_e \right)_{L^2} + \left( q^2 F(t)^2 D_e \mathbf{n} \cdot \mathbf{n} \widetilde{M}_{0,e}, V_e \right)_{L^2} = 0 \quad \text{in } \mathcal{D}'(]0, T[) \\ \left( \partial_t \widetilde{M}_{0,c}, V_c \right)_{L^2} + \left( \eta_c(\widetilde{M}_{0,c} - \widetilde{M}_{0,e}), V_c \right)_{L^2} = 0 \quad \text{in } \mathcal{D}'(]0, T[) \end{array} \right.$$

We introduce for almost every  $t \in ]0, T[$ , the bilinear form  $a(\cdot; \cdot, \cdot)$  defined, for every  $(U, V) \in X^2$  by

$$\begin{aligned} a(t; U, V) &= (D_e \nabla U_e, \nabla V_e)_{L^2} + (\eta_e(U_e - U_c), V_e)_{L^2} - (\imath q F(t) D_e U_e \mathbf{n}, \nabla V_e)_{L^2} \\ &+ (\imath q F(t) D_e \nabla U_e \cdot \mathbf{n}, V_e)_{L^2} + (q^2 F(t)^2 D_e \mathbf{n} \cdot \mathbf{n} U_e, V_e)_{L^2} + (\eta_c(U_c - U_e, V_c)_{L^2}. \end{aligned}$$

As  $f \in L^\infty(]0, T[)$  (and consequently  $F \in L^\infty(]0, T[)$ ), for every  $(U, V) \in X^2$ ,  $t \mapsto a(t; U, V)$  is measurable. Moreover, we get, using Cauchy-Schwarz inequality

$$\begin{aligned} |a(t; U, V)| &\leq \|D_e\| \|\nabla U_e\|_{L^2} \|\nabla V_e\|_{L^2} + \|D_e\| \|q\| F \|U_e\|_{L^2} \|\nabla V_e\|_{L^2} \\ &\quad + \|D_e\| \|q\| F \|U_e\|_{L^2} \|\nabla U_e\|_{L^2} \|V_e\|_{L^2} \|D_e\| q^2 \|F\|_{L^\infty(]0, T[)}^2 \|U_e\|_{L^2} \|V_e\|_{L^2} \\ &\quad + \eta_e (\|U_e\|_{L^2} + \|U_c\|_{L^2}) \|V_e\|_{L^2} + \eta_c (\|U_e\|_{L^2} + \|U_c\|_{L^2}) \|V_c\|_{L^2} \end{aligned}$$

which globally gives

$$|a(t; U, V)| \leq C(\eta_e, \eta_c, \|D_e\|, q, F) \|U\|_X \|V\|_X,$$

for some constant  $C(\eta_e, \eta_c, \|D_e\|, q, F) > 0$ , and if we endow  $X$  with its natural Hilbert space norm

$$\|U\|_X^2 = \|U_e\|_{H^1}^2 + \|U_c\|_{L^2}^2.$$

Next, we have,

$$\begin{aligned} a(t; U, U) &= (D_e \nabla U_e, \nabla U_e)_{L^2} - iqF(t) (U_e D_e \mathbf{n}, \nabla U_e)_{L^2} + iqF(t) (D_e \nabla U_e \cdot \mathbf{n}, U_e)_{L^2} \\ &\quad + q^2 F(t)^2 D_e \mathbf{n} \cdot \mathbf{n} (U, U)_{L^2} + \eta_e (U_e - U_c, U_e)_{L^2} + \eta_c (U_c - U_e, U_c)_{L^2}. \end{aligned}$$

Then,

$$\begin{aligned} \Re(a(t; U, U)) &\geq \sigma^- \|\nabla U_e\|_{L^2}^2 + q^2 F(t)^2 \sigma^- \|U_e\|_{L^2}^2 - 2q|F(t)| \|D_e\| \|\nabla U\|_{L^2} \|U\|_{L^2} \\ &\quad + \eta_e (U_e - U_c, U_e)_{L^2} + \eta_c (U_c - U_e, U_c)_{L^2}, \end{aligned}$$

where  $\sigma^-$  is such that  $D_e \xi \cdot \xi \geq \sigma^- \|\xi\|^2$  for any  $\xi \in \mathbb{R}^d$ , which exists as  $D_e$  is positive definite. Using Young's inequality, we get

$$\begin{aligned} \Re(a(t; U, U)) &\geq \frac{\sigma^-}{2} \|\nabla U_e\|_{L^2}^2 + q^2 F(t)^2 \left( \sigma^- - \frac{2\|D_e\|^2}{\sigma^-} \right) \|U_e\|_{L^2}^2 \\ &\quad + \left( \eta_e - \frac{\eta_e + \eta_c}{2} \right) \|U_e\|_{L^2}^2 + \left( \eta_c - \frac{\eta_e + \eta_c}{2} \right) \|U_c\|_{L^2}^2. \end{aligned}$$

Then, for any  $\lambda > 0$ , such that for some fixed  $\delta > 0$  and almost every  $t \in ]0, T[$ ,

$$\lambda + q^2 F(t)^2 \left( \sigma^- - \frac{2\|D_e\|^2}{\sigma^-} \right) - \frac{\eta_e + \eta_c}{2} \geq \delta > 0,$$

(such a  $\lambda$  exists as  $f \in L^\infty(]0, T[)$ ),

$$\Re(a(t; U, U)) + \lambda \|U\|_{L^2}^2 \geq \min \left( \frac{\sigma^-}{2}, \delta \right) \|U\|_X^2.$$

Then, Lion's theorem (see for instance [9, Chapter XVIII]) ensures the existence and uniqueness of the solution of the variational problem

$$\left\{ \begin{array}{l} \frac{d}{dt} \langle \widetilde{M}(t), V \rangle_{X', X} + a(t; \widetilde{M}(t), V) = 0 \quad \text{in } \mathcal{D}'(]0, T[), \quad \forall V \in X \\ \widetilde{M}(0) = M_{init}. \end{array} \right. \quad (3.28)$$

Now, in order to get estimates (3.26) and (3.27), we use  $V = \widetilde{M}(t)$  as a test function, which is possible since  $\widetilde{M} \in W(0, T, X)$ . We integrate over time, and get

$$\frac{1}{2} \|\widetilde{M}_{0,e}(t)\|_{L^2}^2 + \frac{1}{2} \|\widetilde{M}_{0,c}(t)\|_{L^2}^2 - \|M_{init}\|_{L^2}^2 + \int_0^t a(s; \widetilde{M}(s), \widetilde{M}(s)) ds = 0$$

Proceeding as in the coercivity proof,

$$\begin{aligned}
& \frac{1}{2} \|\widetilde{M}_{0,e}(t)\|_{L^2}^2 + \frac{1}{2} \|\widetilde{M}_{0,c}(t)\|_{L^2}^2 + \frac{\sigma^-}{2} \int_0^t \|\nabla \widetilde{M}_{0,e}(s)\|_{L^2}^2 ds + q^2 \sigma^- \int_0^t F(s)^2 \|\widetilde{M}_{0,e}(s)\|_{L^2}^2 ds \\
& + \eta_e \int_0^t \|\widetilde{M}_{0,e}(s)\|_{L^2}^2 ds + \eta_c \int_0^t \|\widetilde{M}_{0,c}(s)\|_{L^2}^2 ds \leq \|M_{init}\|_{L^2}^2 + \frac{2\|D_e\|^2 q^2}{\sigma^-} \int_0^t F(s)^2 \|\widetilde{M}_{0,e}(s)\|_{L^2}^2 ds \\
& \quad + \frac{\eta_e + \eta_c}{2} \int_0^t \|\widetilde{M}_{0,e}(s)\|_{L^2}^2 ds + \frac{\eta_e + \eta_c}{2} \int_0^t \|\widetilde{M}_{0,c}(s)\|_{L^2}^2 ds
\end{aligned} \tag{3.29}$$

using Young's inequality. In particular,

$$\|\widetilde{M}(t)\|_H^2 \leq 2\|M_{init}\|_{L^2}^2 + \int_0^t \left( \frac{4\|D_e\|^2 q^2}{\sigma^-} F(s)^2 + (\eta_e + \eta_c) \right) \|\widetilde{M}(s)\|_H^2 ds +$$

Then, using Gronwall's lemma,

$$\begin{aligned}
\|\widetilde{M}(t)\|_H & \leq \sqrt{2} \|M_{init}\|_{L^2} \exp \left( \frac{2\|D_e\|^2 q^2}{\sigma^-} \int_0^t F(s)^2 ds + (\eta_e + \eta_c)t \right) \\
& \leq 2\|M_{init}\|_{L^2} \exp \left( \frac{2\|D_e\|^2 q^2 \|F\|_{L^\infty(]0,T])}^2}{\sigma^-} + \eta_e + \eta_c \right) t
\end{aligned}$$

which implies (3.26). To prove (3.27), we notice that (3.29) yields

$$\int_0^t \|\nabla \widetilde{M}(s)\|_H^2 ds \leq \frac{2}{\sigma^-} \|M_{init}\|_{L^2}^2 + \int_0^t \left( \frac{4\|D_e\|^2 q^2}{\sigma^-} F(s)^2 + (\eta_e + \eta_c) \right) \|\widetilde{M}(s)\|_H^2 ds.$$

Using (3.26), we deduce

$$\int_0^t \|\nabla \widetilde{M}(s)\|_H^2 ds \leq \frac{2}{\sigma^-} \|M_{init}\|_{L^2}^2 \left( 1 + \exp \left[ \left( \frac{4\|D_e\|^2 q^2 \|F\|_{L^\infty(]0,T])}^2}{\sigma^-} + \eta_e + \eta_c \right) t \right] \right),$$

which corresponds with (3.27). Finally, using the well-known injection  $W(0, T, H^1) \hookrightarrow C^0(0, T, L^2)$ , it is now a classical exercise to prove rigorously the equivalence between problems (3.28) and (3.25).  $\square$  Now, the multiplication by  $e^{i q \mathbf{n} \cdot \mathbf{x} F(t)}$  and its inverse  $e^{-i q \mathbf{n} \cdot \mathbf{x} F(t)}$  clearly defines a bijection between  $W(0, T, X)$  with its natural norm

$$\|U\|_{W(0,T,X)}^2 = \|U\|_{L^2(0,T,X)}^2 + \|\partial_t U\|_{L^2(0,T,X')}^2$$

and the space

$$W^{q,f}(0, T, X) = \left\{ U \in L^2(0, T, X) \mid \partial_t^{q,f} U \in L^2(0, T, X') \right\},$$

where  $\partial_t^{q,f}$  denotes the operator  $\partial_t^{q,f} = \partial_t + i q \mathbf{n} \cdot \mathbf{x} f(t)$ , if we endow  $W^{q,f}(0, T, X)$  with the norm

$$\|U\|_{W^{q,f}(0,T,X)}^2 = \|U\|_{L^2(0,T,X)}^2 + \|\partial_t^{q,f} U\|_{L^2(0,T,X')}^2.$$

Thus, the previous result dictates the following notion of solution for problem (3.20):

A variational solution of problem (3.20) is an element  $M_0 = (M_{0,e}, M_{0,c})$  of  $W^{q,f}(0, T, X) \cap$

$C^0(0, T, L^2(\mathbb{R}^d))^2$  such that, for any  $V \in X$ , we have

$$\left\{ \begin{array}{l} \left\langle \partial_t^{q,f} M_{0,e}, V_e \right\rangle_{H^{-1}, H^1} + (D_e \nabla M_{0,e}, V_e)_{L^2(\mathbb{R}^d)} + (\eta_e(M_{0,e} - M_{0,c}), V)_{L^2(\mathbb{R}^d)} = 0 \quad \text{in } \mathcal{D}'(]0, T[) \\ \left( \partial_t^{q,f} M_{0,c}, V_c \right)_{L^2} + (\eta_c(M_{0,c} - M_{0,e}), V)_{L^2(\mathbb{R}^d)} = 0 \quad \text{in } \mathcal{D}'(]0, T[) \\ M_{0,e}(0) = M_{init} \quad \text{in } \mathbb{R}^d \\ M_{0,c}(0) = M_{init} \quad \text{in } \mathbb{R}^d \end{array} \right. \quad (3.30)$$

We immediately deduce from theorem 1

**THEOREM 2.** *Let  $f \in L^\infty(0, T)$  and  $M_{init} \in L^2(\Omega)$ . There exists a unique variational solution  $M = (M_{0,e}, M_{0,c}) \in W^{q,f}(0, T, X) \cap C^0(0, T, L^2(\mathbb{R}^d))^2$  to problem (3.20). If  $\Omega$  is bounded, then the previous result also holds true if we replace  $H^1(\Omega)$  by  $H_0^1(\Omega)$  and we supplement equations (3.20) by homogeneous Dirichlet boundary conditions for  $M_{0,e}$  on  $\partial\Omega$ . In that case, the proof can be conducted directly on  $M_0$ , as the problem on a bounded domain does not involve unbounded coefficients anymore.*

**REMARK 1.** *In the cases where  $D_c$  is also positive definite matrix (which corresponds to the presence of elongated cells or axons), one has to rather consider system (3.19) and Theorem 2 holds true in this case with  $H = L^2(\Omega) \times L^2(\Omega)$  and  $X = H^1(\Omega) \times H^1(\Omega)$ . From the solution to (3.20) one can built an approximation of the magnetization as*

$$M_\varepsilon \approx \frac{|Y_e|}{|Y|} M_{0,e} + \frac{|Y_c|}{|Y|} M_{0,c}$$

This formally account for

$$M_\varepsilon \simeq M_{0,e} \quad \text{in } \Omega_e^\varepsilon \quad \text{and} \quad M_\varepsilon \simeq M_{0,c} \quad \text{in } \Omega_c^\varepsilon.$$

More precisely one can prove that under the hypothesis of Theorem 2,

$$M_\varepsilon \rightharpoonup \frac{|Y_e|}{|Y|} M_{0,e} + \frac{|Y_c|}{|Y|} M_{0,c} \quad \text{weakly in } L^2(0, T, L^2(\mathbb{R}^d)) \quad (3.31)$$

The proof is given in [6] and uses the periodic unfolding method [5], extended to the time dependent cases.

**4. An ODE model.** In this section, we give more details about the measured signal in a dMRI experiment and we explain how to use the model introduced in the previous section to obtain an approximation to the signal in a simple manner. In practice, the diffusion-encoding magnetic field gradient has a time profile that satisfies, at the echo time  $T_E$ ,

$$\int_0^{T_E} f(t) dt = 0 \quad (4.1)$$

and the signal is measured at  $t = T_E$ . The measured signal is given by

$$S_\varepsilon(q, \mathbf{n}) = \int_{\mathbb{R}^d} M_\varepsilon(\mathbf{x}, T_E) d\mathbf{x}.$$

Then, it is natural to define the approximate signal by:

$$S(q, \mathbf{n}) = \int_{\mathbb{R}^d} M_e(\mathbf{x}, T_E) + M_c(\mathbf{x}, T_E) d\mathbf{x}$$

where we have set

$$M_e := \frac{|Y_e|}{|Y|} M_{0,e} \quad \text{and} \quad M_c := \frac{|Y_c|}{|Y|} M_{0,c}. \quad (4.2)$$

**4.1. A coupled ODE model for dMRI's signals.** Let us denote

$$m_e^0 = \int_{\mathbb{R}^d} M_e(\mathbf{x}, 0) d\mathbf{x}, \quad m_c^0 = \int_{\mathbb{R}^d} M_c(\mathbf{x}, 0) d\mathbf{x} \quad \text{and} \quad m^0 = \int_{\mathbb{R}^d} M_e(\mathbf{x}, 0) + M_c(\mathbf{x}, 0) d\mathbf{x}.$$

These initial moments will naturally appear in the following and are of great interest for the inverse problem since

$$\theta_e = \frac{m_e^0}{m_0} = \frac{|Y_e|}{|Y|} \quad \text{and} \quad \theta_c = \frac{m_c^0}{m_0} = \frac{|Y_c|}{|Y|}$$

represents respectively the extra-cellular volume fraction and the intra-cellular volume fraction. We now establish that the signal obtained from solving (3.20) can be equivalently obtained by solving a simpler system of coupled ODEs.

**THEOREM 3.** *Under the hypothesis of Theorem 2, if we further assume that  $f$  satisfies (4.1) and assume that the Fourier transform of  $M_{init}$  is continuous in the neighborhood of the origin, then the signal  $S(q, \mathbf{n})$  is well defined and can be computed as*

$$S(q, \mathbf{n}) = m(T_E)$$

where  $m = m_e + m_c$ , and  $(m_e, m_c) \in C^1(0, T_E)^2$  is the unique solution of

$$\begin{cases} \frac{dm_e}{dt} + q^2 \sigma_e \left( \int_0^t f(s) ds \right)^2 m_e + \eta_e (m_e - m_c) = 0, \\ \frac{dm_c}{dt} + \eta_c (m_c - m_e) = 0, \\ m_e(0) = m_e^0 \text{ and } m_c(0) = m_c^0, \end{cases} \quad (4.3)$$

where  $\sigma_e := D_e \mathbf{n} \cdot \mathbf{n}$ .

*Proof.* Let  $(M_{0,e}, M_{0,c})$  be the unique solution of (3.20) in  $C^0(0, T_E, H) \cap W^{q,f}(0, T_E, X)$ . We set again

$$\widetilde{M}_e(\mathbf{x}, t) = M_e(\mathbf{x}, t) e^{i q \mathbf{n} \cdot \mathbf{x} \int_0^t f(s) ds} \quad \text{and} \quad \widetilde{M}_c(\mathbf{x}, t) = M_c(\mathbf{x}, t) e^{i q \mathbf{n} \cdot \mathbf{x} \int_0^t f(s) ds}$$

Then, as we have seen before, we obtain the system of equations for  $\widetilde{M}_e$  and  $\widetilde{M}_c$  (using the symmetry of  $D_e$ ),

$$\begin{cases} \frac{\partial \widetilde{M}_e}{\partial t} - \operatorname{div}(D_e \nabla \widetilde{M}_e) + 2i q D_e \nabla \widetilde{M}_e \cdot \mathbf{n} \left( \int_0^t f(s) ds \right) \\ \quad + q^2 D_e \mathbf{n} \cdot \mathbf{n} \left( \int_0^t f(s) ds \right)^2 \widetilde{M}_e + \eta_e (\widetilde{M}_e - \widetilde{M}_c) = 0 & \text{in } \Omega \times ]0, T_E[, \\ \frac{\partial \widetilde{M}_c}{\partial t} + \eta_c (\widetilde{M}_c - \widetilde{M}_e) = 0 & \text{in } \Omega \times ]0, T_E[, \end{cases}$$

with the initial conditions

$$\widetilde{M}_e(\cdot, 0) = \theta_e M_{init}, \quad \widetilde{M}_c(\cdot, 0) = \theta_c M_{init} \quad \text{in } \Omega.$$

We denote by  $\mathcal{M}_e$  and  $\mathcal{M}_c$  the Fourier transform with respect to the space variable of respectively  $\widetilde{M}_e$  and  $\widetilde{M}_c$  and denote the dual variable  $\xi$ . Applying the Fourier transform to the system of equations satisfied by  $\widetilde{M}_e$  and  $\widetilde{M}_c$  yields

$$\begin{cases} \frac{\partial \mathcal{M}_e}{\partial t} + D_e \xi \cdot \xi \mathcal{M}_e - 2q D_e \xi \cdot \mathbf{n} \mathcal{M}_e \left( \int_0^t f(s) ds \right) \\ \quad + q^2 D_e \mathbf{n} \cdot \mathbf{n} \left( \int_0^t f(s) ds \right)^2 \mathcal{M}_e + \eta_e (\mathcal{M}_e - \mathcal{M}_c) = 0 & \text{in } \Omega \times ]0, T_E[, \\ \frac{\partial \mathcal{M}_c}{\partial t} + \eta_c (\mathcal{M}_c - \mathcal{M}_e) = 0 & \text{in } \Omega \times ]0, T_E[. \end{cases}$$

From our hypothesis,  $\mathcal{M}_e(\cdot, 0)$  and  $\mathcal{M}_c(\cdot, 0)$  are continuous functions. We therefore deduce from classical standard results on parametric first order linear differential systems that  $\mathcal{M}_e$  and  $\mathcal{M}_c$  belong to  $C^1([0, T_E], C^0(\Omega))$ . We set

$$m_e(t) := \mathcal{M}_e(0, t) \quad \text{and} \quad m_c := \mathcal{M}_c(0, t),$$

which can be formally written as

$$m_e(t) = \int_{\mathbb{R}^d} \widetilde{M}_e(\mathbf{x}, t) d\mathbf{x} \quad \text{and} \quad m_c(t) = \int_{\mathbb{R}^d} \widetilde{M}_c(\mathbf{x}, t) d\mathbf{x} \quad (4.4)$$

where the integrals has to be understood as duality pairing in the distributional sense. We observe that, for  $\xi = 0$ , the above system of equations directly implies

$$\begin{cases} \frac{dm_e}{dt} + q^2 \sigma_e \left( \int_0^t f(s) ds \right)^2 m_e + \eta_e(m_e - m_c) = 0, \\ \frac{dm_c}{dt} + \eta_c(m_c - m_e) = 0, \end{cases}$$

with  $\sigma_e = D_e \mathbf{n} \cdot \mathbf{n}$ . Finally, for the signal we have for  $\alpha = e, c$ , using  $\int_0^{T_E} f(s) ds = 0$ ,

$$\int_{\mathbb{R}^d} M_\alpha(\mathbf{x}, T_E) d\mathbf{x} = \int_{\mathbb{R}^d} \widetilde{M}_\alpha(\mathbf{x}, T_E) e^{-iq\mathbf{n} \cdot \mathbf{x}} \int_0^{T_E} f(s) ds d\mathbf{x} = \int_{\mathbb{R}^d} \widetilde{M}_\alpha(\mathbf{x}, T_E) = m_\alpha(T_E)$$

which concludes the proof.  $\square$

Our ODE model is reminiscent of the so-called Karger model [12]. In fact, the latter can be seen as a simplified version of our model when the pulse duration  $\delta$  is very small compared to the interval between the two pulses:  $\delta \ll \Delta$ . However this assumption is not always realistic in medical imaging due to hardware limitations. In addition, the Karger model is obtained heuristically, whereas we derived the ODE model of (4.3) more rigorously from the microscopic Bloch-Torrey PDE.

**REMARK 2.** *Indeed, for the general case where  $D_c \neq 0$ , the system (4.3) has to be replaced with*

$$\begin{cases} \frac{dm_e}{dt} + q^2 \sigma_e \left( \int_0^t f(s) ds \right)^2 m_e + \eta_e(m_e - m_c) = 0, \\ \frac{dm_c}{dt} + q^2 \sigma_c \left( \int_0^t f(s) ds \right)^2 m_c + \eta_c(m_c - m_e) = 0, \\ m_e(0) = m_e^0 \text{ and } m_c(0) = m_c^0, \end{cases} \quad (4.5)$$

where  $\sigma_c = D_c \mathbf{n} \cdot \mathbf{n}$ .

**4.2. Numerical validation of the ODE model.** Now we will compare our macroscopic model to the two compartments microscopic model, using simplified geometries and biologically reasonable parameters for the intrinsic diffusion coefficients and the membrane permeability. Simulations on more complex and realistic cellular geometries will be the subject of a future paper.

We will take the commonly used PGSE diffusion encoding sequence in (2.1). By construction, we have:

$$\int_0^{T_E} f(t) dt = 0$$

and for simplicity we will take  $T_E = \delta + \Delta$ .

The dMRI signal can be measured for several values of  $q$ ,  $\delta$ ,  $\Delta$  and directions  $\mathbf{n}$ . We will consequently denote by  $S(q, \delta, \Delta, \mathbf{n})$  the signal to emphasize this dependency and also normalize

this signal by dividing it by  $\int_{\mathbb{R}^d} M_{init} d\mathbf{x}$ . It is common in the dMRI community not to display  $S(q, \delta, \Delta, \mathbf{n})$  as a function of  $q$ , but as a function of the so called b-value

$$b(q) := q^2 \int_0^{\Delta+\delta} \left( \int_0^t f(s) ds \right)^2 dt = q^2 \delta^2 \left( \Delta - \frac{\delta}{3} \right)$$

To understand why the quantity is used, notice that in the case of a single Bloch-Torrey equation in  $\mathbb{R}^d$  with a constant diffusion tensor  $D$ ,

$$\begin{cases} \frac{\partial M}{\partial t} + i\mathbf{q}\mathbf{n} \cdot \mathbf{x} f(t)M - \text{div}_{\mathbf{x}}(D\nabla_{\mathbf{x}}M) = 0 & \text{in } \mathbb{R}^d \times ]0, T_E[, \\ M(\cdot, 0) = M_{init} & \text{in } \mathbb{R}^d, \end{cases}$$

the Fourier transform  $\hat{M}$  is solution of

$$\begin{cases} \frac{\partial \hat{M}}{\partial t} - f(t)\mathbf{q}\mathbf{n} \cdot \nabla_{\xi} \hat{M} + \xi^T D \xi \hat{M} = 0 & \text{in } \mathbb{R}^d \times ]0, T_E[, \\ \hat{M}(\cdot, 0) = \hat{M}_{init} & \text{in } \mathbb{R}^d. \end{cases}$$

This problem can easily be solved using the method of characteristics, and we obtain

$$\hat{M}(\xi, t) = \hat{M}_{init} \left( \xi + \mathbf{q}\mathbf{n} \int_0^t f(s) ds \right) \exp \left( -D \left( \xi + \mathbf{q}\mathbf{n} \int_s^t f(\mu) d\mu \right) ds \cdot \int_0^t \left( \xi + \mathbf{q}\mathbf{n} \int_s^t f(\mu) d\mu \right) \right).$$

Then, since  $\int_{\mathbb{R}^d} M(\mathbf{x}, \Delta + \delta) d\mathbf{x} = \hat{M}(0, \Delta + \delta)$  we can get in this particular case an expression for the corresponding normalized signal

$$\tilde{S}(q, \delta, \Delta, \mathbf{n}) := \left( \int_{\mathbb{R}^d} M(\mathbf{x}, \Delta + \delta) d\mathbf{x} \right) / \left( \int_{\mathbb{R}^d} M_{init}(\mathbf{x}) d\mathbf{x} \right) = \hat{M}(0, \Delta + \delta) / \hat{M}_{init}(0)$$

that simplifies into, using  $\int_0^{\Delta+\delta} f(s) ds = 0$ ,

$$\tilde{S}(q, \delta, \Delta, \mathbf{n}) = \exp \left( -q^2 D \mathbf{n} \cdot \mathbf{n} \int_0^{\Delta+\delta} \left( \int_0^s f(\mu) d\mu \right)^2 ds \right) = \exp \left( -(D \mathbf{n} \cdot \mathbf{n}) b(q) \right).$$

We then observe that  $\log(\tilde{S}(q, \delta, \Delta, \mathbf{n}))$  is a linear function of the b-value and the slope of this linear function is  $-(D \mathbf{n} \cdot \mathbf{n})$ , which gives access to the coefficients of the tensor  $D$  by varying  $\mathbf{n}$ .

We now provide some numerical results using biologically reasonable values for the intrinsic diffusion coefficients and the membrane permeability on some simple geometries. We compare the signal obtained using the system of ODEs (4.3) to the signal obtained by solving the two-compartment periodic PDE model (2.4).

Since (2.4) is a problem on  $\mathbb{R}^d$ , we cannot numerically solve it for arbitrary initial condition. For the numerical simulations we will rather consider the case of constant  $M_{init}$ . It can be easily shown that a solution of (2.4) is quasi-periodic in space, with period  $\varepsilon$  and quasi-periodic coefficient  $\exp(-i\varepsilon q_i \int_0^t f(s) ds)$  in each direction  $e_i$ . Thus, if we extend the definition of a normalized signal as

$$S_{\varepsilon} = \lim_{N \rightarrow \infty} \frac{\int_{\Omega_N} M_{\varepsilon}(\mathbf{x}, T_E) d\mathbf{x}}{\int_{\Omega_N} M_{init}(\mathbf{x}) d\mathbf{x}},$$

where  $\Omega_N$  denotes the union of  $N$  cells, one gets, for constant  $M_{init}$ ,

$$S_{\varepsilon} = \frac{1}{M_{init} |Y_{\varepsilon}|} \int_{Y_{\varepsilon}} M_{\varepsilon}(\mathbf{x}, T_E) d\mathbf{x},$$

where  $Y_{\varepsilon}$  denotes a given periodicity cell. Then one can reduce the computations to only one periodicity cell with quasiperiodicity condition. For the homogenized model we indeed equivalently

extend the definition of the normalized signal  $S$  similarly to  $S_\varepsilon$  by replacing  $M_\varepsilon$  with the homogenized field  $M$ . Even if the case of constant initial conditions does not enter into the previous theoretical framework (initial conditions is not  $L^2(\mathbb{R}^d)$ ) one can easily verify that if we denote  $(m_e, m_c)$  the solution of (4.3) associated with the initial conditions

$$m_e(0) = \theta_e \text{ and } m_c(0) = \theta_c,$$

then

$$M_e(\mathbf{x}, t) = M_{init} m_e(t) e^{-i\mathbf{q}\cdot\mathbf{x}} \int_0^t f(s) ds \quad \text{and} \quad M_c(\mathbf{x}, t) = M_{init} m_c(t) e^{-i\mathbf{q}\cdot\mathbf{x}} \int_0^t f(s) ds,$$

correspond, through (4.2), with  $(M_{0,e}, M_{0,c})$  solution of (3.20). One then easily check that the normalized signal is still given by  $S(q, \delta, \Delta, \mathbf{n}) = m_e(T_E) + m_c(T_E)$ .

We test two situations in dimension 2, for simplicity. One is a single circular biological cell of radius  $R_m$  placed at the center of the periodicity cell, for several values of  $\Delta$ , with a gradient direction  $e_x$ . The second one is the case of several circular biological cells of variable radii, for gradient directions  $e_x$  and  $e_y$ . We solve the ODE model (4.3), along with the periodic reference model (2.4) on a very refined mesh. Both computations are performed using `FreeFem++` [14].

A comparison of the signals obtained from the exact and approximate models is displayed on Figures 4.1 and 4.2, where the values of the model parameters are indicated. These values are chosen close to the values used often in the literature [22, 10] for dMRI numerical simulations. We can see on these figures that the ODE model (4.3) provides an excellent approximation when modeling dMRI signals for all four diffusion times  $\Delta = 5, 15, 25, 35ms$ . In particular, this approximate model accurately reproduces the 'curvature' of the signal: the obtained signals with the two models are indeed not a single exponential (the log is not a straight line), as it would be in the case of single Bloch-Torrey equation without membranes. This phenomenon, well-known in the medical imaging community, can be reinterpreted from the ODE model: it is the fact that we have two coupled equations that induces this memory-like effect (see the end of Section 3). As both the fact that we have two equations and that they are coupled come from the scaling we have chosen for the permeability, we can thus conclude that the non-monoexponential behavior of the dMRI signal attenuation is the result of the influence of cell membranes, which acts as barriers (as our scaling corresponds to a low permeability).

**5. The inverse problem : retrieving macroscopic properties of tissues from dMRI measurements.** Now that we have checked that our model accurately reproduces the signal, the natural idea is to check whether we can retrieve the coefficients of our simplified model from the measured signals, i.e. if we can solve the inverse problem of finding the unknown coefficients  $\beta = (\eta_e, \eta_c, D_e, m_{e,0}, m_{c,0})$ . These coefficients are of great practical importance. Indeed, from initial moments, we can recover the cellular volume fractions, thus giving information on the concentration of cells, or their potential swelling. The coupling coefficients are also a way to obtain information on the permeability of cellular membranes, which is a very difficult quantity to measure in practice, while the homogenized tensor can give some information on the orientation of nerve fibers in the brain, for instance.

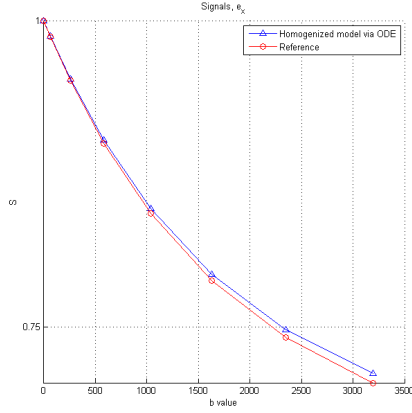
Let  $(\mathcal{S}_i)_{1 \leq i \leq N_{exp}}$  be a set of measures. For instance, we can take :

$$\mathcal{S}_i = S(q_i, \delta_i, \Delta_i, \mathbf{n}_i)$$

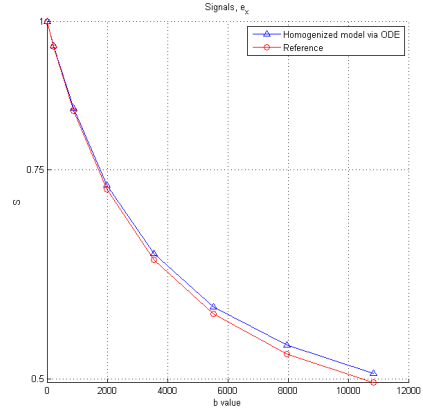
where  $S$  is the signal from the homogenized model, or:

$$\mathcal{S}_i = S_\varepsilon(q_i, \delta_i, \Delta_i, \mathbf{n}_i)$$

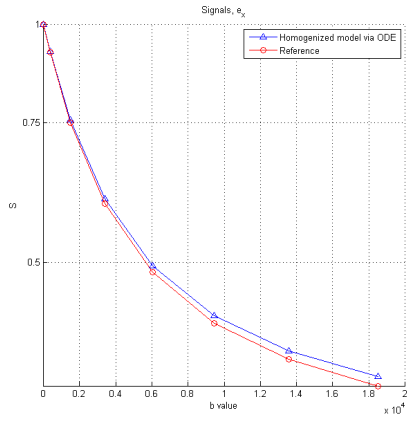
where we use measures obtained from the two compartment heterogeneous model.



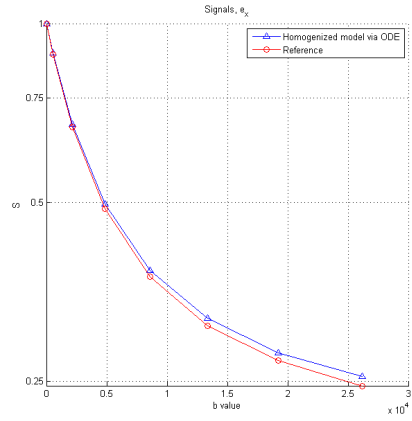
(a)  $\Delta = 5ms$ .



(b)  $\Delta = 15ms$ .



(c)  $\Delta = 25ms$ .



(d)  $\Delta = 35ms$ .

FIG. 4.1. Normalized signals for a single circular biological cell of radius  $R_m = 0.49\mu m$  in a periodicity cell of  $1\mu m^3$ , with  $\sigma_e = 3 \times 10^{-3} mm^2/s$ ,  $\sigma_c = 1.6 \times 10^{-3} mm^2/s$ ,  $\kappa = 5 \times 10^{-5} mm/ms$ ,  $\delta = 3.5ms$ ,  $\mathbf{n} = \mathbf{e}_x$ , for various  $\Delta$ .

As our model is only approximate, if we do not use exact data (which will of course be the case in practice), we cannot hope to find  $\beta = (\eta_e, \eta_c, D_e, m_{e,0}, m_{c,0})$  such that :

$$\mathcal{S}_i = S(q_i, \delta_i, \Delta_i, \mathbf{n}_i)$$

for all  $1 \leq i \leq N_{exp}$ . This is why the natural problem is to minimize the distance between the experimental signals and the theoretical one. A natural choice is thus to solve the classical least squares problem : find  $\beta = (\eta_e, \eta_c, D_e, m_{e,0}, m_{c,0})$  which minimizes the functional :

$$G(\beta) = \sum_{i=1}^{N_{exp}} |S(q_i, \delta_i, \Delta_i, \mathbf{n}_i) - \mathcal{S}_i|^2$$

This least squares problem can be tackled numerically using one of the many methods of the literature for solving inverse problems using least squares. As our purpose here is to illustrate the feasibility of this inverse problem, we have chosen to use the well tested interior-reflective Newton method described in [8] and [7] and implemented in `Matlab` under the name `lsqnonlin`. To generate the measures, we have used the model parameters :

$$\sigma_e = 3 \times 10^{-3} mm^2/s, \quad \sigma_c = 1.6 \times 10^{-3} mm^2/s, \quad \kappa = 5 \times 10^{-5} mm/ms,$$

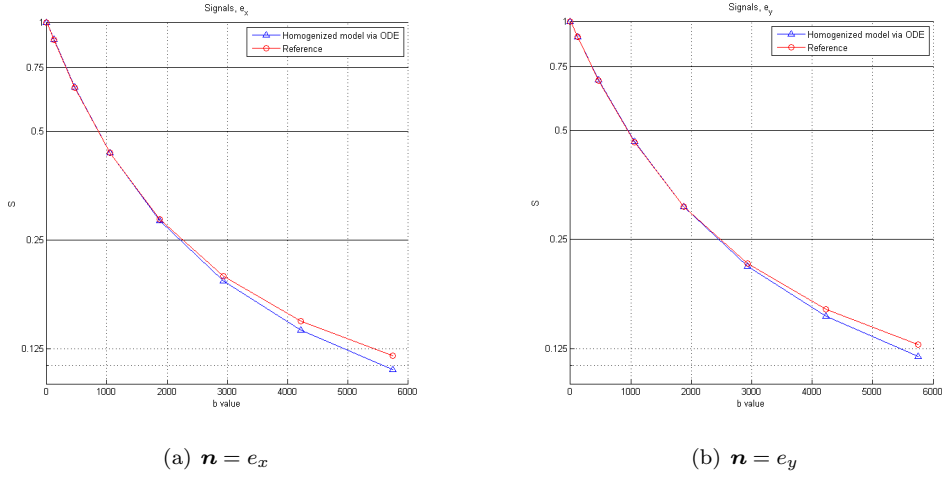


FIG. 4.2. Normalized signals and the periodicity cell, with  $\sigma_e = 3 \times 10^{-3} mm^2/s$ ,  $\sigma_c = 1.6 \times 10^{-3} mm^2/s$ ,  $\kappa = 5 \times 10^{-5} mm/ms$ ,  $\delta = 3.5ms$ ,  $\Delta = 5ms$ ,  $\mathbf{n} = e_x$  and  $e_y$ .

and computed the signals from models (4.3) and (2.4) for directions  $e_x$  and  $e_y$ , for  $q_i = 0.000015 \times i \times 10^6 (mm \times ms)^{-1}$ ,  $i = 0..25$ , and for  $(\delta, \Delta) = (3.5, 5), (3.25, 7.5), (3, 10), (2.75, 12.5)ms$ . We now provide results for the two situations described in the previous section.

First, we consider the case of a single circular biological cell of radius  $R_m = 0.49$ . To solve our minimization problem, we use a random starting set of parameters  $\beta_0$  that are at most 50% different in the  $l^\infty$  norm from the exact set of parameters  $\beta^*$  we are looking for. We provide results for several values of  $\beta_0$  on Table 5.1 (we display  $(\eta_e, \eta_c, \theta_c, D_e(0, 0), D_e(0, 1), D_e(1, 0), D_e(1, 1))$  in each entry of the table, as it is equivalent in our case to knowing  $\theta_c$  and  $m_0 = S(0, \delta_i, \Delta_i, \mathbf{n}_i)$  or  $m_{e,0}$  and  $m_{c,0}$ ).

We see from these results that, as can be expected, the estimated parameters are closer to the real, homogenized values, when we use the signals from model (4.3) than when we use the non-homogenized signal coming from model (2.4). Indeed, the modeling error, corresponding to the fact that (4.3) is an approximation of (2.4) and thus the signals coming from these two models, while being close, are not equal, can be reinterpreted as the fact that (2.4) provides "noisy" data when we try to solve the inverse problem for (4.3).

It can also be observed on Table 5.1 that the quality of the estimated coefficients seems to depend on our initial guess. To limit the effect of this arbitrary choice, we have solved the inverse problem for several initial guesses, and took the values of the estimated coefficients that correspond to the smallest residual. Results are displayed on Table 5.2. We see on Table 5.2 that the results are in this case more robust, and that we obtained a quite good approximation of our homogenized coefficients.

<i>Type of data</i>	<i>Initial guess</i>	<i>Homogenization</i>	<i>Inversion</i>
<i>Non-homogenized signal <math>\mathcal{S}_\varepsilon</math></i>	0.00072825	0.00062439	0.00083039
	0.00021223	0.00020424	0.00024101
	0.9028	0.75352	0.87943
	0.0011	0.00090387	0.0011329
	$2.2630e - 09$	$3.3371e - 09$	$2.263e - 09$
	$2.0958e - 09$	$3.3371e - 09$	$2.0958e - 09$
	0.0014	0.00090397	0.0011329
<i>Non-homogenized signal <math>\mathcal{S}_\varepsilon</math></i>	0.00041904	0.00062439	0.0004921
	0.00010878	0.00020424	0.0002121
	0.7996	0.75352	0.7187
	0.0012	0.00090387	0.00083655
	$3.9017e - 09$	$3.3371e - 09$	$3.9017e - 09$
	$2.3041e - 09$	$3.3371e - 09$	$2.3041e - 09$
	0.00078547	0.00090397	0.00083658
<i>Homogenized signal <math>\mathcal{S}</math></i>	0.00075905	0.00062439	0.00067182
	0.00024167	0.00020424	0.00020651
	0.7882	0.75352	0.75021
	0.00073191	0.00090387	0.00094546
	$2.8164e - 09$	$3.3371e - 09$	$2.8164e - 09$
	$4.1110e - 09$	$3.3371e - 09$	$4.111e - 09$
	0.00064833	0.00090397	0.00094556
<i>Homogenized signal <math>\mathcal{S}</math></i>	0.00062060	0.00062439	0.00088715
	0.00016355	0.00020424	0.00022292
	0.9699	0.75352	0.90318
	0.0010	0.00090387	0.0011188
	$3.3381e - 09$	$3.3371e - 09$	$3.3381e - 09$
	$3.2792e - 09$	$3.3371e - 09$	$3.2792e - 09$
	0.00066511	0.00090397	0.0011189

TABLE 5.1

*Numerical inversion for the case of a single circular biological cell, for two randomly chosen initial sets  $\beta_0$*

To further improve the results, one could wonder if we could use some of the link between the parameters. In particular, notice that we have:

$$\frac{\eta_e}{\eta_c} = \frac{\theta_c}{\theta_e} = \frac{\theta_c}{1 - \theta_c} \quad \text{and} \quad m_{c,0} = \theta_c m_0$$

and consequently :

$$m_{c,0} = \frac{\eta_e m_0}{\eta_e + \eta_c}$$

Thus, we can eliminate  $m_{c,0}$  in our inversion process. We reproduce the above study in this case. We display on Table 5.3 the inversion from one randomly chosen set of initial guesses, while on Table 5.4 we again display the values of the estimated parameters that correspond to the smallest residual from several randomly chosen initial guesses. We see on these two Tables that the estimated parameters are much closer to the exact homogenized values when we use this constraint, even when using a single randomly chosen initial guess (the results being of course still better when we perform several estimations). Thus, it seems that adding this constraint can improve parameter estimation through solving the inverse problem.

<i>Type of data</i>	<i>Initial guesses</i>	<i>Homogenization</i>	<i>Inversion</i>
<i>Non-homogenized signal <math>\mathcal{S}_\varepsilon</math></i>	10	0.00062439	0.00084568
		0.00020424	0.00023061
		0.75352	0.60243
		0.00090399	0.0011663
		$7.3873e - 09$	$7.2782e - 09$
		$7.3873e - 09$	$1.0272e - 08$
		0.00090393	0.0011661
<i>Non-homogenized signal <math>\mathcal{S}_\varepsilon</math></i>	15	0.00062439	0.00064367
		0.00020424	0.00022337
		0.75352	0.68816
		0.00090399	0.00097322
		$7.3873e - 09$	$7.8142e - 09$
		$7.3873e - 09$	$6.0091e - 09$
		0.00090393	0.00097307
<i>Non-homogenized signal <math>\mathcal{S}_\varepsilon</math></i>	20	0.00062439	0.00063403
		0.00020424	0.0002231
		0.75352	0.6957
		0.00090399	0.00096379
		$7.3873e - 09$	$6.8829e - 09$
		$7.3873e - 09$	$1.1063e - 08$
		0.00090393	0.00096364
<i>Homogenized signal <math>\mathcal{S}</math></i>	10	0.00062439	0.00081316
		0.00020424	0.00022011
		0.75352	0.95444
		0.00090399	0.001063
		$7.3873e - 09$	$7.3733e - 09$
		$7.3873e - 09$	$1.0349e - 08$
		0.00090393	0.001063
<i>Homogenized signal <math>\mathcal{S}</math></i>	15	0.00062439	0.00062805
		0.00020424	0.00020354
		0.75352	0.73866
		0.00090399	0.0009066
		$7.3873e - 09$	$9.3574e - 09$
		$7.3873e - 09$	$9.9634e - 09$
		0.00090393	0.00090654

TABLE 5.2  
*Numerical inversion for the case of a single circular biological cell, using several initial sets  $\beta_0$*

Finally, we display on Table 5.5 the results obtained for the periodicity cell of Figure 4.2, where there are 4 circular biological cells of different sizes, with the parameters :

$$\sigma_e = 3 \times 10^{-3} mm^2/s, \quad \sigma_c = 1.6 \times 10^{-3} mm^2/s, \quad \kappa = 5 \times 10^{-5} mm/ms,$$

and measures obtained for the same input parameters,  $q$ ,  $\mathbf{n}$ ,  $\delta$ ,  $\Delta$ , as before. We use the constraint and perform several initial guesses, taking again the parameters corresponding to the smallest residual. We see that even in this more complicated situation, the inverse problem still gives good estimates of the parameters.

**6. Conclusion.** We have proposed a new macroscopic model for the signal obtained from dMRI experiments. This new model, obtained through homogenization of the two-compartment

<i>Type of data</i>	<i>Initial guess</i>	<i>Homogenization</i>	<i>Inversion</i>
<i>Non-homogenized signal <math>\mathcal{S}_\varepsilon</math></i>	0.00059987	0.00062439	0.00056023
	0.00030261	0.00020424	0.00021833
		0.75352	0.71957
	0.00059331	0.00090387	0.00089672
	$4.5236e - 09$	$3.3371e - 09$	$4.5236e - 09$
	$3.8202e - 09$	$3.3371e - 09$	$3.8202e - 09$
	0.00079212	0.00090397	0.00089675
<i>Non-homogenized signal <math>\mathcal{S}_\varepsilon</math></i>	0.00043140	0.00062439	0.0005243
	0.00018959	0.00020424	0.00021462
		0.75352	0.70955
	0.00088762	0.00090387	0.00086532
	$2.0711e - 09$	$3.3371e - 09$	$2.0711e - 09$
	$3.6358e - 09$	$3.3371e - 09$	$3.6358e - 09$
	0.00065645	0.00090397	0.00086535
<i>Homogenized signal <math>\mathcal{S}</math></i>	0.00073690	0.00062439	0.00069693
	0.00019858	0.00020424	0.00020925
		0.75352	0.76908
	0.00086721	0.00090387	0.00096295
	$3.9885e - 09$	$3.3371e - 09$	$3.9885e - 09$
	$2.5031e - 09$	$3.3371e - 09$	$2.5031e - 09$
	0.00070501	0.00090397	0.00096305
<i>Homogenized signal <math>\mathcal{S}</math></i>	0.00032186	0.00062439	0.00055099
	0.00030310	0.00020424	0.00019789
		0.75352	0.73575
	0.00060304	0.00090387	0.00084013
	$2.0230e - 09$	$3.3371e - 09$	$2.023e - 09$
	$2.9113e - 09$	$3.3371e - 09$	$2.9113e - 09$
	0.00063108	0.00090397	0.00084022

TABLE 5.3

Numerical inversion for the case of a single circular biological cell, for two randomly chosen initial sets  $\beta_0$ , using the constraint  $\theta_c = \frac{\eta_e}{\eta_e + \eta_c}$

Bloch-Torrey equation, accurately reproduces the memory effects commonly observed experimentally, and explains it as the influence of cellular membranes on the diffusion of water. This model is a good candidate for obtaining in practice quantitative macroscopic information on the probed tissue through solving the inverse problem on the ODE model. Numerical implementation of this approach for more complex cell geometries will be the subject of a future article. Similarly, the complete mathematical justification of the homogenization process and the study of the uniqueness of the solution of the inverse problem will be the subject of another article.

#### REFERENCES

- [1] T. ARBOGAST. *Gravitational forces in dual-porosity systems: I. model derivation by homogenization*. Transport in Porous Media, volume 13: pp. 179–203, 1993.
- [2] T. ARBOGAST. *Gravitational forces in dual-porosity systems: II. computational validation of the homogenized model*. Transport in Porous Media, volume 13: pp. 205–220, 1993.
- [3] A. BENSOUSSAN, J. LIONS, AND G. PAPANICOLAOU. *Asymptotic analysis for periodic structures, vol. 5 de Studies in Mathematics and its Applications*. North-Holland Publishing Co., Amsterdam, 1978.
- [4] H. BREZIS. *Analyse fonctionnelle, théorie et applications*. Masson, Paris, 1983.
- [5] D. CIORANESCU, A. DAMLAMIAN, AND G. GRISO. *The periodic unfolding method in homogenization*. SIAM J.

<i>Type of data</i>	<i>Initial guesses</i>	<i>Homogenization</i>	<i>Inversion</i>
<i>Non-homogenized signal <math>\mathcal{S}_\varepsilon</math></i>	10	0.00062439	0.00055388
		0.00020424	0.00021904
		0.75352	0.7166
		0.00090399	0.00088566
		$7.3873e - 09$	$8.128e - 09$
		$7.3873e - 09$	$4.9688e - 09$
		0.00090393	0.00088551
<i>Homogenized signal <math>\mathcal{S}</math></i>	10	0.00062439	0.00058975
		0.00020424	0.00020164
		0.75352	0.74521
		0.00090399	0.00087136
		$7.3873e - 09$	$1.035e - 08$
		$7.3873e - 09$	$1.0633e - 08$
		0.00090393	0.0008713

TABLE 5.4

Numerical inversion for the case of a single circular biological cell, using several initial sets  $\beta_0$ , under the constraint  $\theta_c = \frac{\eta_e}{\eta_e + \eta_c}$

<i>Type of data</i>	<i>Initial guesses</i>	<i>Homogenization</i>	<i>Inversion</i>
<i>Non-homogenized signal <math>\mathcal{S}_\varepsilon</math></i>	10	0.00047981	0.00032008
		0.00046232	0.00038455
		0.50928	0.45425
		0.001948	0.0017607
		$7.7789e - 06$	$8.1847e - 06$
		$7.7789e - 06$	$4.1457e - 06$
		0.0017534	0.0015911
<i>Homogenized signal <math>\mathcal{S}</math></i>	10	0.00047981	0.00045812
		0.00046232	0.00045389
		0.50928	0.50232
		0.001948	0.0019139
		$7.7789e - 06$	$9.5453e - 06$
		$7.7789e - 06$	$6.6441e - 06$
		0.0017534	0.0017228

TABLE 5.5

Numerical inversion for the case of the periodicity cell of Figure 4.2, using several initial sets  $\beta_0$ , under the constraint  $\theta_c = \frac{\eta_e}{\eta_e + \eta_c}$

- Math. Anal. 40, pp. 1585-1620, 2012.
- [6] J. COATLÉVEN. *Mathematical justification of macroscopic models for diffusion mri through the periodic unfolding method*. Preprint, 2012.
- [7] T. COLEMAN AND Y. LI. *On the convergence of reflective newton methods for large-scale nonlinear minimization subject to bounds*. Mathematical Programming, Vol. 67, Number 2, pp. 189-224, 1994.
- [8] T. COLEMAN AND Y. LI. *An interior, trust region approach for nonlinear minimization subject to bounds*. SIAM Journal on Optimization, Vol. 6, pp. 418-445, 1996.
- [9] R. DAUTRAY AND J.-L. LIONS. *Mathematical analysis and numerical methods for science and technology, volume 5 : evolution problems*. Springer, 1993.
- [10] K. D. HARKINS, J.-P. GALONS, T. W. SECOMB, AND T. P. TROUARD. *Assessment of the effects of cellular tissue properties on adc measurements by numerical simulation of water diffusion*. Magn. Reson. Med.,

- volume 62 (6): pp. 1414–1422, 2009. ISSN 1522-2594. URL <http://dx.doi.org/10.1002/mrm.22155>.
- [11] M. A. HORSFIELD AND D. K. JONES. *Applications of diffusion-weighted and diffusion tensor mri to white matter diseases, a review*. NMR Biomed., volume 15 (7-8): pp. 570–577, 2002. ISSN 1099-1492. URL <http://dx.doi.org/10.1002/nbm.787>.
- [12] J. KARGER, H. PFEIFER, AND W. HEINIK. *Principles and application of self-diffusion measurements by nuclear magnetic resonance*. Advances in magnetic resonance, volume 12: pp. 1–89, 1988.
- [13] D. LE BIHAN AND H. JOHANSEN-BERG. *Diffusion mri at 25: Exploring brain tissue structure and function*. NeuroImage, volume 61 (2): pp. 324–341, 2012. ISSN 1053-8119. URL <http://www.sciencedirect.com/science/article/pii/S1053811911012857>.
- [14] O. PIRONNEAU, F. HECHT, AND J. MORICE. *freefem++*, [www.freefem.org/](http://www.freefem.org/).
- [15] W. S. PRICE. *Pulsed-field gradient nuclear magnetic resonance as a tool for studying translational diffusion: Part 1. basic theory*. Concepts Magn. Reson., volume 9 (5): pp. 299–336, 1997. ISSN 1099-0534. URL [http://dx.doi.org/10.1002/\(SICI\)1099-0534\(1997\)9:5<299::AID-CMR2>3.0.CO;2-U](http://dx.doi.org/10.1002/(SICI)1099-0534(1997)9:5<299::AID-CMR2>3.0.CO;2-U).
- [16] D. SCHNAPAUFF, M. ZEILE, M. B. NIEDERHAGEN, B. FLEIGE, P.-U. TUNN, B. HAMM, AND O. DUDECK. *Diffusion-weighted echo-planar magnetic resonance imaging for the assessment of tumor cellularity in patients with soft-tissue sarcomas*. J. Magn. Reson. Imaging, vol. 29, no. 6, pp. 1355–1359, 2009.
- [17] E. O. STEJSKAL AND J. E. TANNER. *Spin diffusion measurements: Spin echoes in the presence of a time-dependent field gradient*. The Journal of Chemical Physics, volume 42 (1): pp. 288–292, 1965. URL <http://dx.doi.org/10.1063/1.1695690>.
- [18] T. SUGAHARA, Y. KOROGI, M. KOCHI, I. IKUSHIMA, Y. SHIGEMATU, T. HIRAI, T. OKUDA, L. LIANG, Y. GE, Y. KOMOHARA, Y. USHIO, , AND M. TAKAHASHI. *Usefulness of diffusion-weighted mri with echo-planar technique in the evaluation of cellularity in gliomas*. J. Magn. Reson. Imaging, vol. 9, no. 1, pp. 53–60, 1999.
- [19] H. TORREY. *Bloch equations with diffusion terms*. Physical Review Online Archive (Prola), volume 104 (3): pp. 563–565, 1956. URL <http://dx.doi.org/10.1103/PhysRev.104.563>.
- [20] Y. TSUSHIMA, A. TAKAHASHI-TAKETOMI, AND K. ENDO. *Magnetic resonance (mr) differential diagnosis of breast tumors using apparent diffusion coefficient (adc) on 1.5-t*. J. Magn. Reson. Imaging, vol. 30, no. 2, pp. 249–255, 2009.
- [21] S. WARACH, D. CHIEN, W. LI, M. RONTAL, AND R. R. EDELMAN. *Fast magnetic resonance diffusion-weighted imaging of acute human stroke*. Neurology, volume 42 (9): pp. 1717–, 1992. URL <http://www.neurology.org/cgi/content/abstract/42/9/1717>.
- [22] J. XU, M. DOES, AND J. GORE. *Numerical study of water diffusion in biological tissues using an improved finite difference method*. Physics in medicine and biology, volume 52 (7): pp. –, 2007. ISSN 0031-9155. URL <http://view.ncbi.nlm.nih.gov/pubmed/17374905>.